Science and Technology of Advanced Materials

ISSN: 1468-6996 (Print) 1878-5514 (Online) Journal homepage: www.tandfonline.com/journals/tsta20

Understanding cross-talk–induced anode slippage in high-voltage mid-Ni NCM/graphite full cells

Seungjae Suk, Namgyu Yoo, Youngsu Lee, Jaesub Kwon, Heeju Ahn, Seungsu Yoo, Jaewoon Lee, Haneul Kim, Joongho Bae, Jongwoo Kim, Chiho Jo, Young-Tae Kim & Kyu-Young Park

To cite this article: Seungjae Suk, Namgyu Yoo, Youngsu Lee, Jaesub Kwon, Heeju Ahn, Seungsu Yoo, Jaewoon Lee, Haneul Kim, Joongho Bae, Jongwoo Kim, Chiho Jo, Young-Tae Kim & Kyu-Young Park (16 May 2025): Understanding cross-talk–induced anode slippage in high-voltage mid-Ni NCM/graphite full cells, Science and Technology of Advanced Materials, DOI: 10.1080/14686996.2025.2502324

To link to this article: https://doi.org/10.1080/14686996.2025.2502324

Publisher: Taylor & Francis & The Author(s). Published by National Institute for Materials Science in partnership with Taylor & Francis Group.

Journal: *Science and Technology of Advanced Materials*

DOI: 10.1080/14686996.2025.2502324

Understanding cross-talk–induced anode slippage in high-voltage mid-Ni NCM/graphite full cells

Seungjae Suk[a], Namgyu Yoo[b], Youngsu Lee[b], Jaesub Kwon[a], Heeju Ahn[c], Seungsu Yoo[c], Jaewoon Lee[d], Haneul Kim[c], Joongho Bae[c], Jongwoo Kim[c], Chiho Jo[c], Young-Tae Kim[a] and Kyu-Young Park[a,b*]

[a]*Department of Materials Science and Engineering, Pohang University of Science and Technology (POSTECH), Pohang 37673, Republic of Korea.*

[b]*Graduate Institute of Ferrous & Eco Materials Technology (GIFT), Pohang University of Science and Technology University, Pohang 37666, Republic of Korea*

[c]*LG Energy Solution, Research Park, Daejeon, 34122, Republic of Korea*

[d]*Department of chemical engineering and Materials Science, University of Minnesota–twin cities, Minneapolis, MN 55455, USA*

[*]Dr. Kyu-Young Park,

Assistant Professor of Graduate Institute of Ferrous & Eco Materials Technology

Department of Materials Science and Engineering

Address: 40, Jigok-ro 212beon-gil, Nam-gu, Pohang-si, Gyeongsangbuk-do, Republic of Korea (Zip code: 37667); Mail: kypark0922@postech.ac.kr;

ORCID: https://orcid.org/0000-0001-9560-8526

ORCID

Seungjae Suk: https://orcid.org/0009-0004-4558-9290

Jaesub Kwon: https://orcid.org/0000-0002-3439-2239

Yong-Tae Kim: https://orcid.org/0000-0001-9232-6558

Kyu-Young Park: https://orcid.org/0000-0001-9560-8526

Understanding Cross-Talk–Induced Anode Slippage in High-Voltage Mid-Ni NCM/Graphite Full Cells

Abstract

While high-voltage operation of mid-Ni layered oxide cathodes in full-cell Li-ion batteries is essential for achieving high energy density, it inevitably accelerates electrode degradation, ultimately resulting in capacity loss. However, the underlying degradation mechanisms under high-voltage conditions remain poorly understood. In this study, we reveal that anode slippage—induced by cross-talk-driven surface degradation—is the dominant factor in capacity fade during high-voltage (4.35 or 4.40 V) cycling of single-crystal mid-Ni layered oxide (SC-NCM)/graphite pouch full-cells. Electrochemical and post-mortem analyses show that, although high-voltage operation induces cathode surface degradation, including lattice oxygen loss and phase transitions, its direct impact on capacity loss is relatively minor compared to that of the anode. Instead, anode degradation is primarily caused by cross-talk effects from cathode Ni dissolution, which promote the accumulation of irreversible organic byproducts—such as LiO*x* and Li_2CO_3—within the solid electrolyte interphase (SEI) layer of the graphite anode. This leads to increased resistance and reduced anode electrochemical activity, disrupting electrode balance and accelerating full-cell capacity fade. These findings highlight the critical role of anode degradation in high-voltage operation and

emphasize the importance of mitigating cross-talk effects. A comprehensive understanding of cross-talk–induced anode slippage is therefore critical for the rational design of high-voltage mid-Ni full-cell systems with long-term durability.

Keywords: lithium-ion batteries; anode slippage; high-voltage cycling; single-crystal mid-Ni NCM; full-cell; cross-talk

Impact statement

This study identifies cross-talk–induced anode slippage as the dominant degradation mechanism in high-voltage mid-Ni NCM/graphite full-cells, emphasizing the need for mechanistic understanding for rational design of durable high-voltage systems.

Introduction

Over the past two decades, lithium-ion battery (LIB) technology has advanced rapidly in parallel with the growth of the electric vehicle (EV) market.[1] Among various battery design parameters, the selection of cathode material chemistry has had a decisive impact on key EV performance metrics such as driving range per charge and cost per battery pack.[2] In line with this need, high-Ni layered oxide cathodes (Ni≥80%, high-Ni NCM) have received significant attention due to their superior energy density, which supports the demand for extended driving range. However, high-Ni NCMs exhibit inferior cycle life due to anisotropic lattice changes during lithium insertion/extraction, which promotes crack propagation along grain boundaries within particles,[3] leading to the formation of rock-salt phases[4] and electrolyte decomposition[5] on newly exposed surfaces. Furthermore, these cathode materials undergo thermal decomposition and oxygen release at relatively low temperatures (~200 ˚C), increasing their vulnerability to thermal runaway.[6,7] These inherent

limitations remain key barriers to the commercialization of high-Ni NCM cathodes. While lithium iron phosphate (LFP) cathodes have recently emerged as viable alternatives for cost-effective battery design that mitigate these issues,[1,8,9] they still present distinct challenges, including lower energy density,[10] poor low-temperature performance[11], and potential supply chain vulnerabilities due to geographically concentrated production capacity.[12]

Single-crystal lithium nickel cobalt manganese oxide (SC-$LiNi_xCo_yMn_{1-x-y}O_2$, $0.4 \leq x \leq 0.6$; hereafter SC mid-Ni NCM) cathodes with medium Ni content (< 60%) have emerged as a promising alternative for moderate-range EVs, offering improved cost flexibility through reduced nickel content compared to high-Ni NCMs.[13,14,15] Notably, SC mid-Ni NCM features lower surface nickel concentration and reduced surface area, substantially limiting electrolyte side reactions compared to high-Ni NCM[16,17] while simultaneously providing superior thermal stability.[18] These properties enable the implementation of space-efficient cell-to-pack architectures despite their layered oxide chemistry, presenting opportunities for substantial cost reduction at the battery pack level and meaningful improvements in practical energy density parameters.[19] Furthermore, SC mid-Ni NCM exhibits operational reliability across a more extensive temperature range than LFP alternatives,[20] factors that have collectively positioned this material as an increasingly prominent candidate for long-lifecycle EV battery applications.[21]

To meet the performance demands for such applications, recent guidelines from the US Council for Automotive Research indicate that SC mid-Ni NCM materials must achieve a pack-level energy density of approximately 235 Wh/kg or higher to remain competitive with internal combustion engine vehicles in the moderate-range EV segment.[22] This target corresponds to roughly 350 Wh/kg at the cell level and requires

a minimum of 800 Wh/kg at the cathode material level. For SC-NCM compositions containing 60% nickel, achieving this level of material energy density necessitates operation at elevated upper cut-off voltages of 4.45 V *vs*. Li/Li^+ (equivalent to 4.40 V in NCM/graphite full-cell configurations), enabling the extraction of a specific capacity of approximately 200 mAh/g.

However, operating at such high voltages introduces critical degradation challenges, particularly for Ni-based layered oxide cathodes. Previous investigations have reported that Ni-based layered oxide cathodes experience complex degradation mechanisms encompassing both mechanical and chemical phenomena during high-voltage operation. Pronounced electrochemical creep and significant lattice strain [23,24] can initiate mechanical fractures and disrupt electrical contact at the electrode–current collector interface. High-voltage cycling also promotes the formation of stacking faults, which can lead to bending and distortion of the cathode microstructure.[26] Concurrently, chemical degradation—particularly surface oxygen release—not only facilitates transition metal dissolution [25] but also reinforces mechanical breakdown through positive feedback mechanisms,[26] further accelerating performance decay during prolonged cycling.

Importantly, such degradation is not confined to the cathode alone but extends to the entire full-cell system. For example, in high-Ni layered oxide/graphite full-cells, cross-talk phenomena have been widely reported, where transition metal ions dissolved from the cathode migrate and induce degradation at the anode.[27] Under high-voltage and high-temperature conditions,[28] Ni ions are known to deposit on the anode surface, thickening the SEI layer,[29] and catalyzing electrolyte decomposition.[30] Such phenomena can be exacerbated under fast charging conditions, which presents a significant challenge for implementing mid-Ni NCM cathodes paired with graphite

anodes in electric vehicle full-cell systems.[31,32] Furthermore, parasitic reactions at the positive electrodes progressively alter the capacity balance between electrodes from their initial alignment, a mechanism known as electrode slippage[35]. While such degradation pathways have been increasingly characterized in high-Ni systems, the interplay between cathode and anode degradation under high-voltage operation in SC mid-Ni NCM/graphite full-cells remains poorly understood. In particular, comprehensive understanding of how each electrode contributes to long-term capacity loss and cell imbalance at elevated voltages is still lacking.

In this study, we systematically investigated the degradation mechanisms in high-voltage (≥4.35 V *vs*. graphite) pouch full-cell configurations using single-crystal mid-Ni layered oxide (SC-NCM6)/graphite cells. While cathode degradation—such as oxygen release, surface phase transitions, and internal cracking—was consistently observed and aligned with previous findings, these changes alone could not account for the observed capacity loss in full-cell systems. Instead, our analysis revealed that anode slippage plays a dominant role in capacity fade during long-term cycling. Crucially, this slippage was not an isolated phenomenon but was directly linked to cross-talk effects originating from cathode degradation. Transition metal dissolution from the cathode, particularly Ni ions, migrated to the anode surface, where it promoted the growth of resistive SEI layers rich in LiO_x and Li_2CO_3 byproducts. This process significantly increased charge transfer resistance and disrupted the "*capacity balance*" between electrodes—effectively limiting the accessible capacity of the cathode due to the constrained lithium storage at the anode. These findings shift the focus of degradation analysis in mid-Ni full-cell systems from cathode instability alone to the interplay between electrodes, highlighting the critical need to mitigate cross-talk pathways to enable stable high-voltage operation.

Methods

Cell specifications and full-cell cycle test conditions

The pouch cell consisted of a SC-NCM6 cathode (~17 mg/cm^2), a graphite anode, a ceramic-coated separator film and a 1.2 M $LiPF_6$ in ethylene carbonate (EC) / ethyl methyl carbonate (EMC) / Diethyl carbonate (DEC) (2:7:1, volume ratio) electrolyte, which was designed for high-voltage long cycling electrochemical performance test. The electrochemical charge/discharge cycling performances of NCM6/graphite pouch full-cells were studied via 0.33 C constant current (CC) charge/discharge cycling on Wonik PNE SC model battery testing system in cell voltage ranges from 2.5-4.35 V and 2.5-4.40 V at 45 ℃. At the 100th and 300th cycles of the full-cell long-term test, reference performance tests (RPT) were implemented by temporarily stopping the test, allowing the pouch cell to cool, and applying two charge-discharge cycles at 0.3 C with the same voltage conditions at 25 °C. Both the pouch cell fabrication and full-cell long-term cycle tests were performed at LG Energy Solution.

Post-mortem characterizations

Pouch-type cells were disassembled in an Ar-filled glove box in the discharge state after cycle tests, and the retrieved electrodes were used for half-cell tests. CR2032-type coin cells were assembled with the cycled electrodes and Li metal as a counter electrode and filled with a fresh electrolyte of 1M $LiPF_6$ in EC / EMC / Dimethyl carbonate (DMC) (1:2:1, volume ratio). The electrolyte was selected with a conventional composition known to be stable below 4.50 V (*vs.* Li/Li$^+$), as the primary objective was to observe the intrinsic state of the cathode and anode materials. For cycled cathodes, 4.35 V and 4.40 V SC-NCM6 half-cells were cycled in the voltage range 2.5-4.40 V and 2.5-4.45 V (*vs.* Li/Li$^+$) at 25 ℃ after 12 h of rest to ensure complete electrolyte wetting. The cell formation conditions include 2 cycles at 0.05 C

with CC charge/discharge protocol within the voltage. Afterward, capacity check was conducted at 0.05 C within the same voltage condition. Prior to synchrotron high resolution powder diffraction (HRPD) and soft X-ray absorption spectroscopy (soft XAS) measurements, cathodes were fully lithiated through constant-current discharging at 0.05 C and a subsequent 6-hour voltage hold at 2.5V. Electrochemical impedance spectroscopy (EIS) was performed over a frequency range from 10^5 Hz to 1 Hz (ZIVE SP2, WonATech). To minimize changes in charge transfer resistance due to SOC, the cells were fully discharged to 2.5 V *vs.* Li/Li^+ at 0.1 C in constant current mode followed by constant voltage mode until the C-rate reached 0.01 C.

Synchrotron HRPD characterizations were performed using the 9B beamline at the Pohang Light Source (PLS-II). Measurements were conducted at 25 ℃ from 15 º to 135 º in 2θ with 0.008 steps, with a monochromatic X-ray wavelength of 1.5461 Å.

O K-Edge and Ni L-Edge soft-XAS were conducted in 10A2 HR PES-II beamline at the Pohang Light Source (PLS-II). The absorption spectra were recorded in total electron yield (TEY) mode. The energies of the detected elements (Ni, O) were calibrated by the reference sample (NiO). The measured data were processed using the Beagle software.[34]

High-resolution transmission electron microscopy images were obtained using a JEOL JEM-2200FS with image spherical aberration corrector at 200 kV, with samples prepared by a focused ion beam (FIB) using a Quanta 3D FEG. The cycled-cathode cross-sectional scanning electron microscopy (SEM) images were also obtained with it.

Time of flight secondary ion mass spectrometry (TOF-SIMS) analysis was performed on an ION-TOF TOF.SIMS 5 spectrometer, equipped with Bi^+ analysis beam and 0.5 kV Cs sputtering beams for probing secondary-ion fragments. X-ray photoelectron spectroscopy (XPS, K-Alpha+, Thermo Fisher Scientific) was performed

using a 200 μm X-ray source and calibrated based on the C 1s peak at 284.5 eV. Graphite anode surface was observed were observed through Field emission SEM (FE-SEM, S-4800, HITACHI). The transition metal content of the separator was quantitatively measured by inductively coupled plasma optical emission spectrometer (ICP-OES Agilent 720, Agilent Technologies Co. Ltd).

Result and discussion

Long-term cycling performance of SC-NCM6/graphite full cells at high-voltage

Figure 1a and Figure S1 illustrate the 600-cycle retention and capacity of SC-NCM6/graphite 40 mAh pouch full-cells when subjected to current application at 0.33 C under upper cut-off voltage conditions of 4.35 V or 4.40 V at 45 ℃. The kinks indicated by arrows in Figure 1a occurred at cycles 100 and 300 due to temporary pause and subsequent resumption of cycling for reference performance test (please refer to the experimental section). At the 4.35 V charging voltage condition, the cell maintained 81.5% capacity retention; however, when the charging voltage was increased to 4.40 V, a rapid decrease in capacity retention was observed from the initial cycling stage, with capacity retention declining below 79.8% after 600 cycles. In terms of discharge capacity, the cell cycled at 4.35 V exhibited an initial value of 198.1 mAh/g, with a capacity decrease of 36.5 mAh/g over 600 cycles. The cell cycled at 4.40 V showed a slightly lower initial discharge capacity of 195.6 mAh/g, despite the expectation of higher de-lithiation at elevated voltages (Figure S1). This observation suggests that degradation may have already initiated during or immediately after the initial formation cycle under the 4.40 V condition, limiting the accessible capacity from the beginning of cycling. After 600 cycles, the total reversible capacity loss at 4.40 V (39.6 mAh/g) exceeded that at 4.35 V. The accelerated degradation of full-cell electrochemical

performance under high-voltage operation aligns with the observation of increased swelling during post-electrochemical evaluation visual inspection of full-cells at higher voltages (Figure S2).

To compare the influences of cathode and anode on full-cell capacity degradation according to the upper cut-off window, differential voltage analysis (dV/dQ) was performed on the discharge curves at the initial cycle and 600 cycle points (Figure 1b-c). Differential voltage analysis can be mathematically modeled as a linear combination of each cathode and anode half-cell based on the relationship equation below, providing a useful non-destructive method to estimate changes in cathode and anode behavior within the full-cell system.[35,36]

$$V_{\text{full-cell}} = V_{\text{cathode}} - V_{\text{anode}} \quad (1)$$

$$\frac{\mathrm{d}V_{\text{full-cell}}}{\mathrm{d}Q} = \frac{\mathrm{d}V_{\text{cathode}}}{\mathrm{d}Q} - \frac{\mathrm{d}V_{\text{anode}}}{\mathrm{d}Q} \quad (2)$$

Figure 1b-c shows the galvanostatic profiles (top) and $-Q_0$dV/dQ plots (bottom) according to capacity per area at the initial cycle and 600th cycle of the full-cell for each upper voltage. The $-Q_0$ factor served to normalize the derivatives based on cell discharge capacity. In these $-Q_0$dV/dQ plots, peaks predominantly arising from the cathode are denoted as $c_{a,b}$ (a: peak number, b: cycle number), while anode-dominant peaks are labeled as $a_{a,b}$. For reference, the characteristic peak deconvolution for the cathode in Figure 1b-c utilized half-cell data from SC-NCM6 (see Figure S3 for detailed explanation). At the beginning of discharge, information about the region where H3-2 phase transition occurs in the cathode (c_1) appears in the $-Q_0$dV/dQ. Peak c_2 corresponds to the M-H1 phase transition of the cathode, while the final a_1 corresponds to the phase transition process between stage 1 and stage 4 of the anode [30,35].

Through dV/dQ plot analysis, it is suggested that electrode slippage of the anode is the direct cause of reversible capacity reduction in the full-cell, and that higher charging voltages lead to greater electrode slippage. Electrode slippage refers to the phenomenon where parasitic side reactions occurring at the anode and/or cathode interfaces progressively alter the capacity balance between electrodes from their initial aligned state.[33],[35],[36] Changes in c_1, c_2, and a_1 peak shifts in $-Q_0dV/dQ$ after 600th cycle compared to the first cycle of the full-cell appear due to reversible capacity loss of each electrode or electrode slippage phenomena.[33] The leftward shift of a_1($a_{1,1}\rightarrow a_{1,600}$, (3)) indicates the degree of anode slippage, while the movements of c_2($c_{2,1}\rightarrow c_{2,600}$, (2)) and c_1($c_{1,1}\rightarrow c_{1,600}$, (1)) are combined results of cathode reversible capacity reduction and anode slippage. Regarding the shift of c_1((1)), both 4.35 V (Figure 1b) and 4.40 V (Figure 1c) full-cells slightly shifted to the left by 0.03 mAh/cm^2 Meanwhile, the change in spacing between c_1 and c_2, which can infer the degree of cathode degradation after cycling, was greater at high voltage, with 0.35 mAh/cm^2 at 4.35 V and 0.41 mAh/cm^2 at 4.40 V. This indirectly confirms that cathode degradation intensifies under high-voltage operation. Analysis of anode slippage((3)) reveals values of 0.57 mAh/cm^2 in the 4.35 V full-cell (Figure 1b) compared to 0.67 mAh/cm^2 in the 4.40 V system (Figure 1c), demonstrating that higher charging voltages substantially accelerate slippage at the anode. This comparison clearly indicates that degradation at the anode, manifested as slippage, plays a more critical role in disrupting full-cell electrochemical balance than cathode-side changes.

To further clarify the dominant contribution of the anode to full-cell capacity loss at elevated cut-off voltages, post-mortem half-cell electrochemical analysis was conducted. After cycling, the full-cells were disassembled, and the cathode/anode electrodes were reassembled into Li-metal half-cells, respectively, to compare their

galvanostatic curves (Figure 1d). To minimize kinetic effects, a low current of 0.05 C was applied, and to simulate the charging situation in full-cell cycling, the system was designed to accommodate charging at a voltage equivalent to the full-cell charging by adding the reduction potential of the graphite anode (0.05 V *vs.* Li/Li^+). Figures 1e-f show the half-cell galvanostatic profiles of SC-NCM6 cathodes before and after long-term evaluation of 4.35 V and 4.40 V full-cells, respectively. The capacity measured in the fresh half-cell at 4.35 V SC-NCM6 was 202.5 mAh/g, with a capacity decrease of 20.2 mAh/g (Figure 1e, (c)) occurring after full-cell cycling. In the 4.40 V SC-NCM6, which had an initial capacity of 205.7 mAh/g, a cathode capacity decrease (Figure 1f, (c)) of 28.0 mAh/g occurred after 600 charge/discharge cycles. In terms of capacity retention, 4.35 V SC-NCM6 and 4.40 V SC-NCM6 showed 90% and 86%, respectively, confirming that the cathode degraded slightly more when operated at 4.40 V. In contrast, for the anode, the reversible capacity decrease (Figure 1g-h, (a)) was about 59 mAh/g under 4.35 V cycling conditions, whereas at 4.40 V, it was approximately twice as much at 110 mAh/g. Given that commercial graphite typically delivers an initial reversible capacity of approximately 350 mAh/g, this indicates that nearly one-third of the capacity becomes inaccessible. These findings confirm that the dominant source of capacity loss under high-voltage operation is not cathode degradation, but severe anode degradation caused by lithium inventory imbalance.

SC-NCM6 cathode degradation behavior during high-voltage cycling

In an ideal full cell with an optimized N/P ratio, increasing the upper cut-off voltage extracts additional capacity from the cathode, while the anode operates within a relatively stable potential range where lithium plating is avoided. Under such conditions, degradation is typically expected to originate from the cathode side. However, the observed acceleration of anode degradation at high voltage indicates that

the anode was unexpectedly impacted, likely due to cross-talk effects originating from the cathode rather than direct electrochemical stress on the anode itself.[28,37,38] This suggests that degradation at the anode is not simply a consequence of high-voltage cycling, but a cathode-induced phenomenon that disrupts the expected electrode stability balance. To investigate the degradation behavior of the SC-NCM6 cathode under high-voltage conditions, TEM and synchrotron-based X-ray analyses—including soft-XAS and HRPD—were conducted to probe structural changes at both the surface and bulk levels (Figure 2).

The breakdown of the layered structure accompanied by oxygen release at the SC-NCM6 surface was confirmed through soft XAS surface analysis. Using synchrotron-soft XAS in TEY mode with a beam size of 300 × 600 μm^2 (Figure 2a), we observed average changes in the chemical bonds around oxygen ions and the electronic structure of transition metal ions in regions approximately 3 nm deep from the SC-NCM6 surface. In the O K-edge spectra, the pre-edge region appearing at 527~534 eV represents O 1s transitions to hybridized TM_{3d}-O_{2p} states.[39] After full-cell cycling, the areal intensity of the pre-edge in the O K-edge decreased, and the signal at 531~532 eV corresponding to the TM-O hybridized state of disordered spinel or rock-salt increased relative to the intensity near 528~530 eV, which corresponds to the TM-O hybridized state of the layered phase (Figure 2a)[39]. Notably, this trend was observed to be more severe in the 4.40 V electrode, indicating that lattice oxygen evolution at the surface occurred more intensely during high-voltage operation.

The reduction of Ni ions near the surface compared to their initial state after cycling was evidenced through Ni L_3-edge TEY mode analysis (Figure 2b). The oxidation state of Ni ions affects their electronic configuration and ligand-field environment, altering multiplet structures and thus the Ni L_3-edge spectral shape; the

smaller the relative ratio of the shoulder peak intensity (I_2) near 852 eV compared to the first peak intensity (I_1) around 850 eV in the L_3-edge, the closer the oxidation state of Ni ions is to '2+' rather than '3+'.[39,40] Indeed, the relative intensity (I_2/I_1) within the Ni L_3-edge peak decreased after full-cell cycling, and this value was smaller in the 4.40 V cycled cathode compared to the 4.35 V cycled cathode (Figure 2c). These findings, consistent with the O K-edge results, further indicate enhanced oxygen release at the cathode surface with increasing cut-off voltage.

Accelerated surface phase transitions and structural collapse at high voltages in SC-NCM6 were confirmed by HR-TEM analysis. Before cycling, the SC-NCM6 surface was confirmed to have a layered structure (Figure S5). After full-cell cycling, the surface commonly existed not as a layered phase but as spinel (*Fd3m*) or cubic structure (*Fm-3m*). A distinctive feature was that in the 4.35 V cathode surface, mixed regions of cubic (I) and spinel (II) structures were frequently observed (Figure 2d), while in the 4.40 V case, only cubic regions (III) were observed (Figure 2e), which has been reported in other ternary layered oxide.[41,42] These surface structural changes might originated from H-transfer reactions facilitated by the Ni lattice, transferring protons from electrolyte solvent molecules to the cathode O lattice, which potentially accelerating transition metal dissolution.[30] Consequently, dissolved transition metals can migrate to and deposit on the anode, promoting surface side reactions. Thus, the observed cathode surface degradation likely contributed significantly to the anode degradation shown in Figure 1g–h.[25]

The acceleration of bulk degradation as well as surface deterioration during high-voltage cycling was observed through HRPD. Among all Bragg peaks, (00l) reflections showed the most significant broadening, with the high-intensity (003) peak used to track structural evolution in SC-NCM6 after cycling (Figure S6). After full-cell

cycling, the (003) peak shifted to the left compared to the pristine cathode in all cycled cathodes, with a greater leftward shift at higher charging voltages. This suggests that despite fully discharging the cathode, internal lithium ions may not have been completely filled due to increased charge transfer resulting from surface degradation. Additionally, examining the FWHM change of the (003) peak, the 4.35 V cycled cathode showed approximately a 12% increase compared to the pristine cathode, while the 4.40 V cycled cathode showed a 103% increase (Figure 2g). From the SEM images of the cross-section of cathode materials after full-cell test in Figure S7, more internal cracks were observed in the 4.40 V cathode compared to the 4.35 V cathode. From the viewpoint of crystallite size, internal cracking of the single-crystal cathode material may have generated smaller crystallites, contributing to the observed peak broadening. Furthermore, a fatigue phase appeared at 2θ=18.40-18.55 ° left of the cycled cathode's (003) peak (Figure S8). Previous studies reported that high-voltage cycling of single-crystal NCM causes chemical inhomogeneity and particle deformation due to repeated lattice expansion and contraction.[43] Higher voltages promote surface oxygen release and accelerate bulk degradation.[26] This irreversible structural deformation during cycling likely contributed to the observed peak broadening, as confirmed by the correlation between integrated intensity of O K pre-edge and FWHM of (003) for SC-NCM6 (Figure S9).

To assess the impact of cathode surface oxygen release and reconstruction on electrochemical activity under high-voltage operation, electrochemical impedance spectroscopy (EIS) analysis was performed. The resistance ($R=R_{SEI} + R_{charge\ transfer}$) measured by EIS of SC-NCM6 after 4.35 V and 4.40 V cycling increased slightly at the higher voltage, with values of 257 Ω and 264 Ω, respectively (Figure 2h). This minor increase can be attributed to more severe oxygen release and surface reconstruction at

the cathode surface under 4.40 V conditions, which is consistent with the greater reduction in reversible cathode capacity observed in Figure 1e–f. Notably, however, the resistance ratio ($R_{4.40\ V}/R_{4.35\ V}$) was only 1.03, whereas the relative increase in anode slippage capacity ($Q_{slippage,4.40\ V}/Q_{slippage,4.35\ V}$) in the full-cell (Figure 1b–c) was substantially higher at 1.18. This indicates that although cathode surface degradation contributes to increased interfacial resistance, its effect on overall full-cell performance is limited compared to the more pronounced impact of anode degradation under high-voltage conditions.

Cross-talk-mediated surface degradation of graphite anode

Cross-talk phenomena originating from the cathode—specifically transition metal dissolution and oxygen release—have been reported to accelerate anode degradation in full-cell systems.[27,28,30] For instance, deposited transition metals on the anode surface can enhance side reactions with the electrolyte, promoting thicker SEI formation, or catalyze hydrogen gas evolution, ultimately accelerating Li inventory loss in full-cells.[29,30] Although graphite anodes are generally considered structurally and electrochemically stable and cyclable in EC / EMC / DEC-based electrolytes (Figure S10),[44-46] the degradation observed in SC-NCM6/graphite full-cells suggests that their interfacial stability can be compromised by cross-talk-induced SEI modifications. To explore these effects in detail, a comprehensive surface analysis of the graphite anode was conducted using SEM, TOF-SIMS, and XPS.[28,46]

SEM imaging revealed that SEI byproducts formed on both 4.35 V and 4.40 V cycled anodes (Figure 3a–b). In the 4.35 V case, they were discretely deposited on individual particles, while at 4.40 V, they formed a continuous and thicker coating (Figure S11). The absence of needle-like byproducts in both cycled anodes, combined with the previous electrochemical analysis results, provides indirect evidence that

graphite anode degradation at high voltage stemmed from SEI layer modifications rather than Li-plating on the surface.[47]

Graphite anode surface degradation was found to intensify with increasing charging voltage, primarily due to transition metal dissolution. This behavior was examined in detail using TOF-SIMS depth profiling to characterize SEI layer evolution on the graphite surface (Figure 3c–d). According to prior studies, the SEI layer typically consists of inorganic species near the surface and organic byproducts at greater depths.[29,30] To capture this structural profile and evaluate transition metal dissolution effects, we monitored signals from Li-based components (LiF_2^-, LiO^-), graphite (C_3^-), and transition metal species (Ni^-, NiF_2^-, MnF_3^-, CoF_3^-), normalized to their maximum intensities across the measured depth range.[28] The depth profiles of LiF_2^-—an indicator of inorganic SEI species—exhibited similar spatial distributions regardless of charging voltage. This suggests that $LiPF_6$ salt decomposition, which generates such inorganic species, is relatively insensitive to voltage variation under these conditions.[46] In contrast, LiO^- signals—representing organic components such as Li_xO and Li_2CO_3—penetrated deeper into the SEI and showed greater intensity at 4.40 V than at 4.35 V (Figure 3e–f). This observation indicates that high-voltage operation accelerates the formation and thickening of organic-rich SEI layers.

Notably, the shaded regions in Figure 3c-d reveal strong overlapping LiO^- and Ni^- profiles, implying a close relationship between transition metal dissolution and organic SEI formation. Such alignment suggests that Ni ions dissolved from the cathode migrate toward the anode and locally catalyze side reactions, thereby enhancing the growth of electrochemically inactive organic species within the SEI.[29] These findings point to a cross-talk mechanism where cathode-derived Ni facilitates SEI thickening, ultimately impairing anode surface properties under high-voltage conditions.

This correlation was further validated by surface-sensitive compositional analyses. XPS Ni 2p spectra showed stronger Ni signals in the 4.40 V-cycled graphite anode than in the 4.35 V case (Figure S12), and ICP-OES analysis of the separator confirmed that Ni content at 4.40 V was more than twice that at 4.35 V (Figure 3g). Consistently, EIS measurements revealed a significant increase in anode resistance, with values of 581 Ω at 4.40 V and 292 Ω at 4.35 V (Figure 3h). These results establish a strong relationship between transition metal accumulation and interfacial impedance increase. Notably, the resistance ratio of the anode ($R_{4.40\ V}/R_{4.35\ V}$) was substantially higher than that of the cathode (1.03), paralleling the capacity loss trends observed in post-mortem half-cell tests—where the anode showed a 110 mAh/g loss, nearly four times that of the cathode (28 mAh/g). Collectively, these findings confirm that reversible capacity reduction in high-voltage full-cells is primarily driven by anode-side degradation, which originates from cathode-induced cross-talk and results in progressive cell balance mismatch.

Conclusion

Single-crystal mid-Ni layered oxide (SC mid-Ni NCM) cathodes have emerged as promising candidates for EV applications, offering suppressed surface side reactions and superior thermal stability compared to high-Ni counterparts. However, high-voltage operation (≥ 4.35 V *vs.* graphite) is required to overcome the limited energy density inherent to their moderate Ni content. Despite growing interest, the full-cell degradation mechanisms of systems incorporating this material under such high-voltage conditions remain poorly understood.

In this study, we reveal that full-cell capacity loss is predominantly governed by anode degradation—specifically anode electrode slippage—induced by cross-talk from

cathode Ni dissolution. During early cycling stages, high-voltage conditions accelerate phase transitions at the cathode surface (from layered to rock-salt), along with lattice oxygen release and transition metal dissolution, particularly of Ni (Figure 4a). Dissolved Ni ions migrate through the electrolyte and deposit on the anode surface, where they promote parasitic side reactions and the continuous growth of organic-rich SEI layers (Figure 4b). This thickened SEI layer significantly increases charge transfer resistance at the anode, reducing its electrochemical activity and leading to a progressive mismatch in electrode capacity. As a result, anode potential slippage occurs, ultimately disrupting cell balance and dominating reversible capacity loss during long-term cycling (Figure 4c).

While previous studies on high-voltage NCM/graphite full cells have primarily focused on cathode degradation or cross-talk in general, our differential voltage analysis and post-mortem evaluation demonstrate that anode-side degradation plays a more decisive role than cathode deterioration. Notably, the sharp rise in interfacial resistance at the anode under high-voltage operation, rather than cathode degradation alone, emerges as the principal factor in full-cell failure. This highlights the importance of addressing anode slippage and preserving electrode balance in the design of stable, high-voltage mid-Ni full-cell systems. This work not only clarifies the dominant role of anode degradation in high-voltage mid-Ni full cells but also provides a framework for future strategies aimed at mitigating cross-talk and preserving long-term cell balance.

Disclosure

The authors report there are no competing interests to declare.

Acknowledgements

This work was supported by LG Energy Solution; 'regional innovation mega project' program through the Korea Innovation Foundation funded by Ministry of Science and ICT under Grant (No. 2023-DD-UP-0032-01); Korea Institute for Advancement of Technology (KIAT) grant funded by the Korea Government (MOTIE) (RS-2024-00419413, HRD Program for Industrial Innovation); the Technology Innovation Program (RS-2024-00459497, Low-Expansion Mid-Nickel Material for Ultra-Long Cycle Life) through the Korea Planning & Evaluation Institute of Industrial Technology (KEIT) funded by the Ministry of Trade, Industry & Energy (MOTIE)

Reference

[1] IEA. Global EV Outlook 2024; https://www.iea.org/reports/global-ev-outlook-2024

[2] Li WD, Erickson EM, Manthiram A, High-nickel layered oxide cathodes for lithium-based automotive batteries. Nat Energy. 2020;5(1):26-34. doi: 10.1038/s41560-019-0513-0

[3] Ryu HH, Yoon CS, Sun YK, et al. Capacity fading of Ni-rich $Li[Ni_xCo_yMn_{1-x-y}]O_2$ ($0.6 \leq x \leq 0.95$) cathodes for high-energy-density lithium-ion batteries: bulk or surface degradation? Chem Mater. 2018;30(3):1155-1163. DOI: 10.1021/acs.chemmater.7b05269

[4] Park NY, Park BC, Sun YK, et al. Degradation mechanism of Ni-rich cathode materials: focusing on particle interior. ACS. Energy Lett. 2022;7(7):2362–2369. DOI: 10.1021/acsenergylett.2c01272

[5] Li WD, Dolocan A, Li JY, et al. Ethylene carbonate-free electrolytes for high-nickel layered oxide cathodes in lithium-ion batteries. Adv Energy Mater. 2019;9(29). doi: 10.1002/aenm.201901152

[6 Cui ZH, Manthiram A. Thermal stability and outgassing behaviors of high-nickel cathodes in lithium-ion batteries. Angew Chem Int Edit. 2023;62(43). doi: 10.1002/anie.202307243

[7] Jo S, Seo S., Kang SK., et al. Thermal runaway mechanism in Ni-rich cathode full cells of lithium-ion batteries: the role of multidirectional crosstalk. Adv Mater. 2024;36(31). doi: 10.1002/adma.202402024

[8] Morris J. Tesla's shift to cobalt-free batteries is its most important move yet. Forbes. 2020 Jul 11.

[9] Takahashi M, Ohtsuka H, Sakurai Y, et al. Confirmation of long-term cyclability and high thermal stability of $LiFePO_4$ in prismatic lithium-ion cells. J Electrochem Soc. 2005;152(5):A899-A904. doi: 10.1149/1.1874693

[10] Manthiram A. A reflection on lithium-ion battery cathode chemistry. Nat Commun. 2020;11(1). doi: 10.1038/s41467-020-15355-0

[11] Rui XH, Jin Y, Chen CH, et al. A comparative study on the low-temperature performance of $LiFePO_4$/C and $Li_3V_2(PO_4)_3$/C cathodes for lithium-ion batteries. J Power Sources. 2011;196(4):2109–2114. doi: 10.1016/j.jpowsour.2010.10.063

[12] Cheng AL, Fuchs ERH, Karplus VJ, et al. Electric vehicle battery chemistry affects supply chain disruption vulnerabilities. Nat Commun. 2024;15(1). doi: 10.5281/zenodo.10607313

[13] Liu TC, Yu L, Liu JJ, et al. Understanding Co roles towards developing Co-free Ni-rich cathodes for rechargeable batteries. Nat Energy. 2021;6(3):277–286. doi: 10.1038/s41560-021-00776-y

[14] Zhang R, Wang CY, Zou PC, et al. Long-life lithium-ion batteries realized by low-Ni, Co-free cathode chemistry. Nat Energy. 2023;8(7):695–702. doi: 10.1038/s41560-023-01267-y

[15] Sim R, Su LS, Manthiram A. A high energy-density, cobalt-free, low-nickel $LiNi_{0.7}Mn_{0.25}Al_{0.05}O_2$ cathode with a high-voltage electrolyte for lithium-metal batteries. Adv Energy Mater. 2023;13(21). doi: 10.1002/aenm.202300096

[16] Zhang F, Lou SF, Li S, et al. Surface regulation enables high stability of single-crystal lithium-ion cathodes at high voltage. Nat Commun. 2020;11(1). doi: 10.1038/s41467-020-16824-2

[17] Klein S, Bärmann P, Fromm O, et al. Prospects and limitations of single-crystal cathode materials to overcome cross-talk phenomena in high-voltage lithium ion cells. J Mater Chem A. 2021;9(12). doi: 10.1039/d0ta11775g

[18] Li KJ, Gao XL, Peng SJ, et al. A comparative study on multidimensional signal evolution during thermal runaway of lithium-ion batteries with various cathode materials. Energy. 2024;300. doi: 10.1016/j.energy.2024.131560

[19] LG Energy Solution. Supplementary stories: the latest insights into battery innovations. LG Energy Solution Newsroom. 2024.
Available at: https://news.lgensol.com/company-news/supplementary-stories/3259/

[20] Rodrigues MTF, Babu G, Gullapalli H, et al. A materials perspective on Li-ion batteries at extreme temperatures. Nat Energy. 2017;2(8). doi: 10.1038/nenergy.2017.108

[22] US DRIVE Electrochemical Energy Storage Technical Team Roadmap. US Council for Automotive Research; 2017.

[23] Bi YJ, Tao JH, Wu YQ, et al. Reversible planar gliding and microcracking in a single-crystalline Ni-rich cathode. Science. 2020;370(6522):1313–1317. doi: 10.1126/science.abc3167

[24] Jousseaume T, Colin JF, Chandesris M, et al. Strain and collapse during lithiation of layered transition metal oxides: a unified picture. Energy Environ Sci. 2024;17(8). doi: 10.1039/d3ee04115h

[25] Song SH, Cho M, Park I, et al. High-voltage-driven surface structuring and electrochemical stabilization of Ni-rich layered cathode materials for Li rechargeable batteries. Adv Energy Mater. 2020;10(23). doi: 10.1002/aenm.202000521

[26] Park KY, Zhu YZ, Torres-Castanedo CG, et al. Elucidating and mitigating high-voltage degradation cascades in cobalt-free $LiNiO_2$ lithium-ion battery cathodes. Adv Mater. 2021;34(3). doi: 10.1002/adma.202106402

[27] Ruff Z, Xu C, Grey CP. Transition metal dissolution and degradation in NMC811-graphite electrochemical cells. J Electrochem. Soc. 2021;168(6). doi: 10.1149/1945-7111/ac0359

[28] Li WD, Liu XM, Xie Q, et al. Long-term cyclability of NCM-811 at high voltages in lithium-ion batteries: an in-depth diagnostic study. Chem Mater. 2020;32(18):7796–7804. doi: 10.1021/acs.chemmater.0c02398.

[29] Xu HY, Li ZP, Liu TC, et al. Impacts of dissolved Ni^{2+} on the solid electrolyte interphase on a graphite anode. Angew Chem Int Ed Engl. 2022;61(30). doi: 10.1002/anie.202202894

[30] Wang XQ, Ren DS, Liang HM, et al. Ni crossover catalysis: truth of hydrogen evolution in Ni-rich cathode-based lithium-ion batteries. Energy Environ Sci. 2023;16(3):1200–1209. doi: 10.1039/d2ee04109j

[31] Cao B, Li T, Zhao W, et al. Correlating rate-dependent transition metal dissolution between structure degradation in Li-rich layered oxides. Small. 2023;19(42). doi: 10.1002/smll.202301834

[32] Suh JH, Han SA, Yang SY, et al. Toward fast-charging and dendritic-free Li growth on natural graphite through intercalation/conversion on MoS_2 nanosheets. Adv Mater. 2025;37(7). doi: 10.1002/adma.202414117

[33] Rodrigues MTF. Addressing limitations of the endpoint slippage analysis. J Electrochem Soc. 2024;171(12). doi: 10.1149/1945-7111/ad9fe3

[34] Park JY, Lee M, Jeong SH, et al. Beagle: a near-edge X-ray absorption fine-structure spectroscopy data processing solution for beamline experiments at Pohang Accelerator Laboratory. J Synchrotron Rad. 2024;31:202–207. doi: 10.1107/s1600577523008755

[35] Bloom I, Jansen AN, Abraham DP, et al. Differential voltage analyses of high-power, lithium-ion cells: technique and application. J Power Sources. 2005;139(1-2):295–303. doi: 10.1016/j.jpowsour.2004.07.021

[36] Dose WM, Xu C, Grey CP, et al. Effect of anode slippage on cathode cutoff potential and degradation mechanisms in Ni-rich Li-ion batteries. Cell Rep Phys Sci. 2020;1(11). doi: 10.1016/j.xcrp.2020.100253

[37] Cañas NA, Einsiedel P, Freitag OT, et al. Operando X-ray diffraction during battery cycling at elevated temperatures: a quantitative analysis of lithium-graphite intercalation compounds. Carbon. 2017;116:255–263. doi: 10.1016/j.carbon.2017.02.002

[38] Kim CS, Jeong KM, Kim K, et al. Effects of capacity ratios between anode and cathode on electrochemical properties for lithium polymer batteries. Electrochim Acta. 2015;155:431–436. doi: 10.1016/j.electacta.2014.12.005

[39] Tian CX, Nordlund D, Xin HLL, et al. Depth-dependent redox behavior of $LiNi_{0.6}Mn_{0.2}Co_{0.2}O_2$. J Electrochem Soc. 2018;165(3):A696–A704. doi: 10.1149/2.1021803jes

[40] Wang HX, Ge PH, Riordan CG, et al. Integrated X-ray L absorption spectra. Counting holes in Ni complexes. J Phys Chem. B. 1998;102(42):8343–8346. doi: 10.1021/jp9821026

[41] Jung SK, Gwon H, Hong J, et al. Understanding the degradation mechanisms of $LiNi_{0.5}Co_{0.2}Mn_{0.3}O_2$ cathode material in lithium-ion batteries. Adv Energy Mater. 2014;4(1). doi: 10.1002/aenm.201300787

[42] Lin F, Markus IM, Nordlund D, et al.. Surface reconstruction and chemical evolution of stoichiometric layered cathode materials for lithium-ion batteries. Nat Commun. 2014;248. doi: 10.1038/ncomms4529

[43] Huang WY, Liu TC, Yu L, et al. Unrecoverable lattice rotation governs structural degradation of single-crystalline cathodes. Science. 2024;384(6698):912–919. doi: 10.1126/science.ado1675

[44] Fong R, Vonsacken U, Dahn JR. Studies of lithium intercalation into carbons using nonaqueous electrochemical cells. J Electrochem Soc. 1990;137(7):2009–2013. doi: 10.1149/1.2086855

[45] Asenbauer J, Eisenmann T, Kuenzel M, et al. The success story of graphite as a lithium-ion anode material—fundamentals, remaining challenges, and recent developments including silicon (oxide) composites. Sustain Energy Fuels. 2020;4(11):5387–5416. doi: 10.1039/d0se00175a

[46] Klein S, Harte P, Henschel J, et al. On the beneficial impact of Li_2CO_3 as electrolyte additive in NCM523 ‖ graphite lithium ion cells under high-voltage conditions. Adv Energy Mater. 2021;11(10). doi: 10.1002/aenm.202003756

[47] Xu K. Nonaqueous liquid electrolytes for lithium-based rechargeable batteries. Chem Rev. 2004;104(10):4303–4417. doi: 10.1021/cr030203g

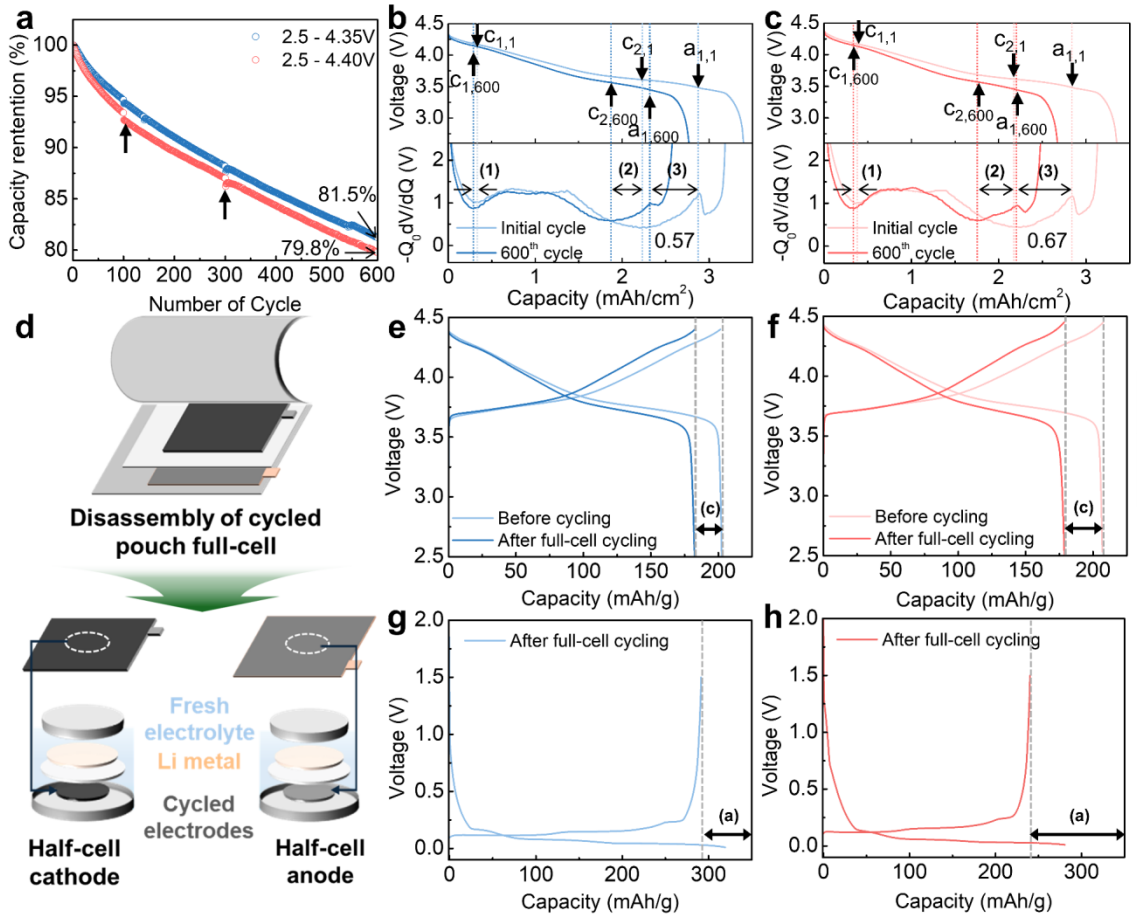

Figure 1. Simultaneous capacity loss of SC-NCM6 cathode and graphite anode in pouch-type full cells during high-voltage long-term cycling. (a) Capacity retention obtained in 2.5-4.35 V(or 4.40 V) at a rate of C/3 after formation cycles. Voltage profiles and differential voltage analysis for (b) 4.35 V and (c) 4.40 V full-cell cycles. (d) Schematic illustration of the post-mortem electrochemical analysis for cycled electrodes; Half-cell charge-discharge curves for the 3rd cycle of SC-NCM6 cathodes retrieved from (e) 4.35 V and (f) 4.40 V full-cells. Half-cell charge-discharge curves for the 1st cycle of graphite anodes retrieved from (g) 4.35 V and (h) 4.40 V full-cells.

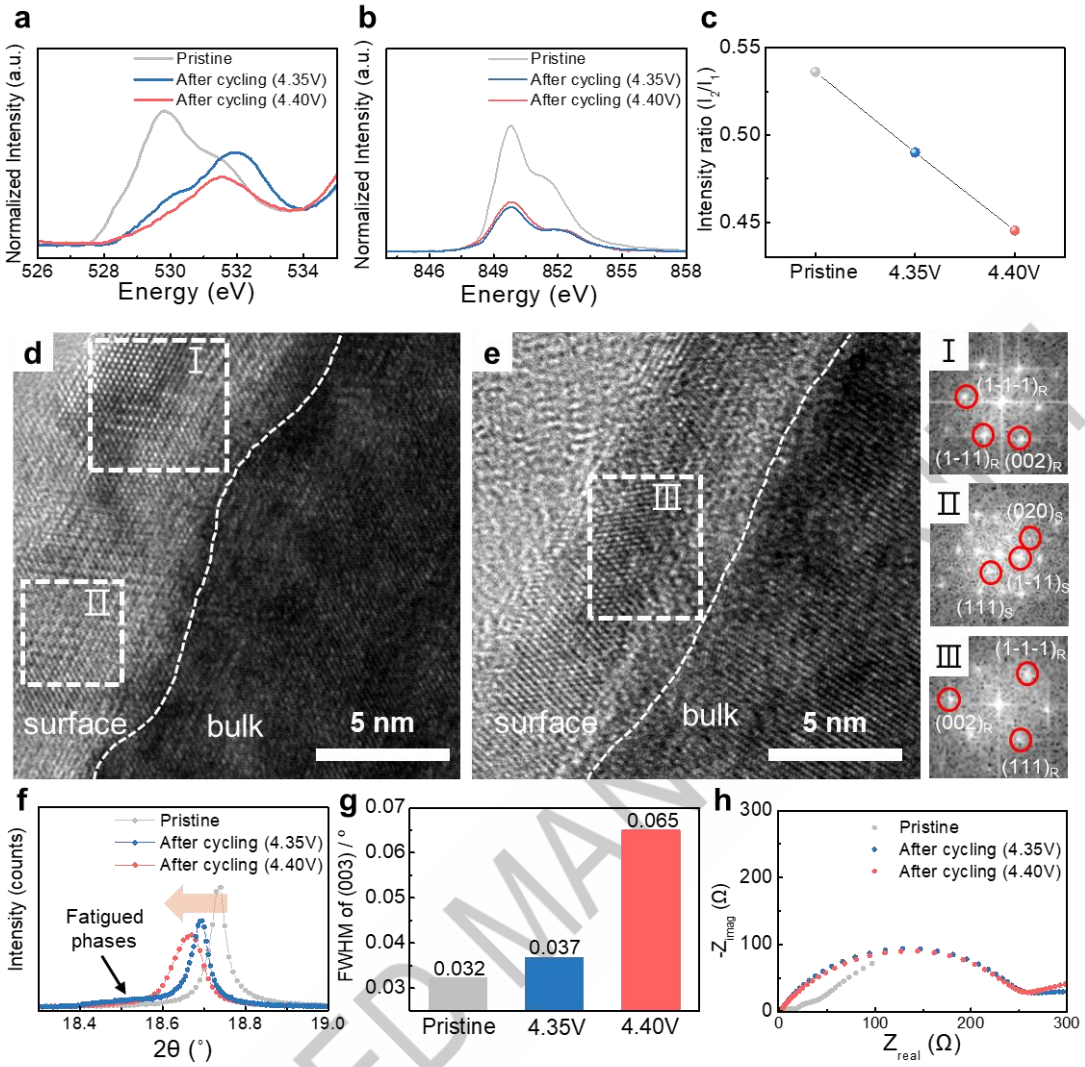

Figure 2. Post-mortem analyses of cycled SC-NCM6 cathodes. (a) Soft XAS O K-edge spectra of the cycled SC-NCM6 cathode. (b) Soft XAS Ni L_3-edge spectra and (c) relative intensity ratio between low energy peak to high energy peak (Ni $L_{3\ low}/L_{3\ high}$). HR-TEM images of the cycled electrodes: (d) cycled at 4.35 V, and (e) cycled at 4.40 V in full-cell cycles. FFT images of the selected area (I, II, III) are labeled by 'I, II, III'. R represents a peak from rocksalt phase; S represents a peak from spinel phase. (f) XRD patterns of Bragg peak (003) from the cycled SC-NCM6. (g) Integrated O K-pre edge peak areas and FWHM of the (003). (h) The EIS profiles of the cycled electrodes.

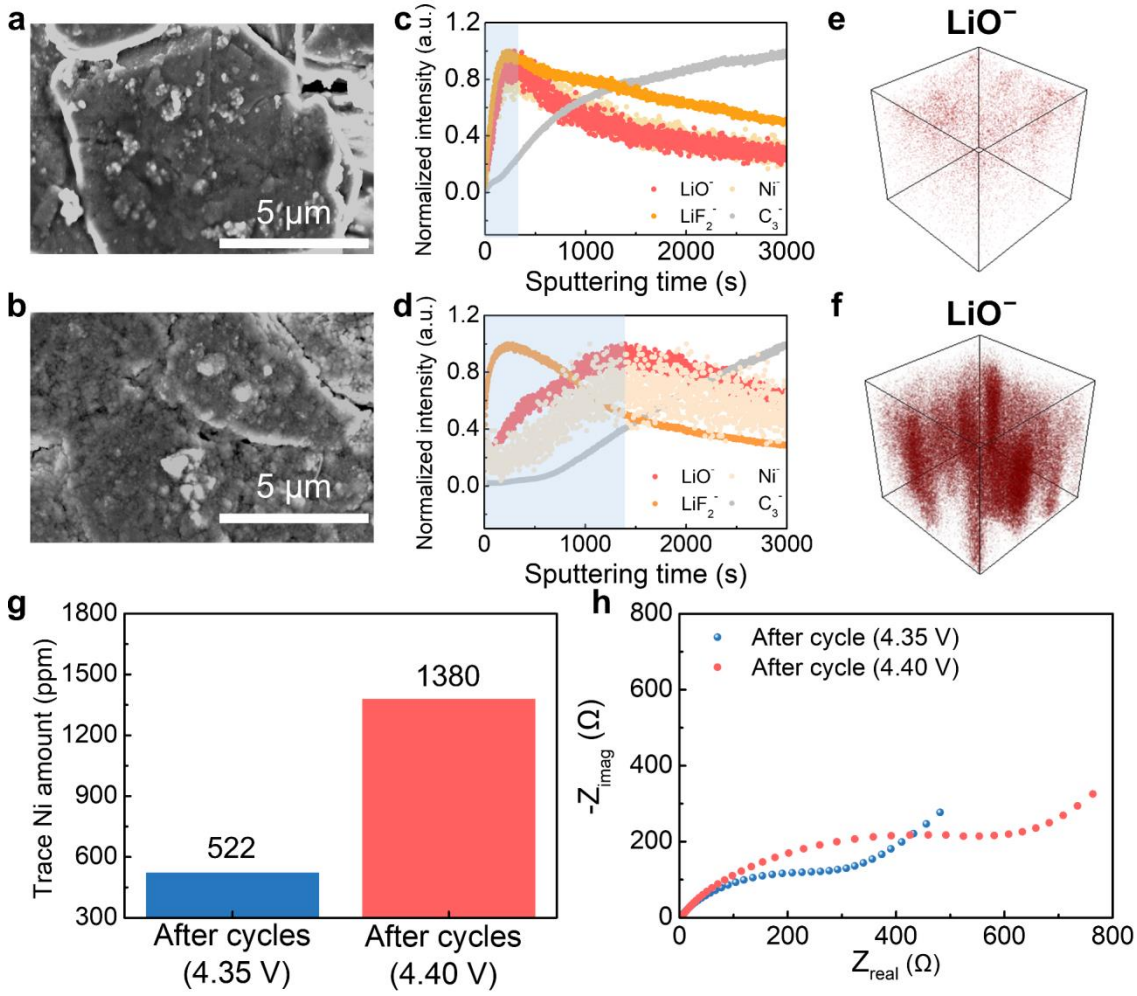

Figure 3. Post-mortem analyses of cycled graphite anodes. SEM images of graphite electrodes operated at (a) 4.35 V and (b) 4.40 V cycling. Normalized TOF-SIMS depth profiles and corresponding 3D LiO^- distribution plots for graphite electrodes cycled at (c, e) 4.35 V and (d, f) 4.40 V. All spectra are normalized to their respective maximum intensities. (g) ICP-OES analysis showing trace Ni content in cycled separators. (h) EIS profiles of the cycled electrodes.

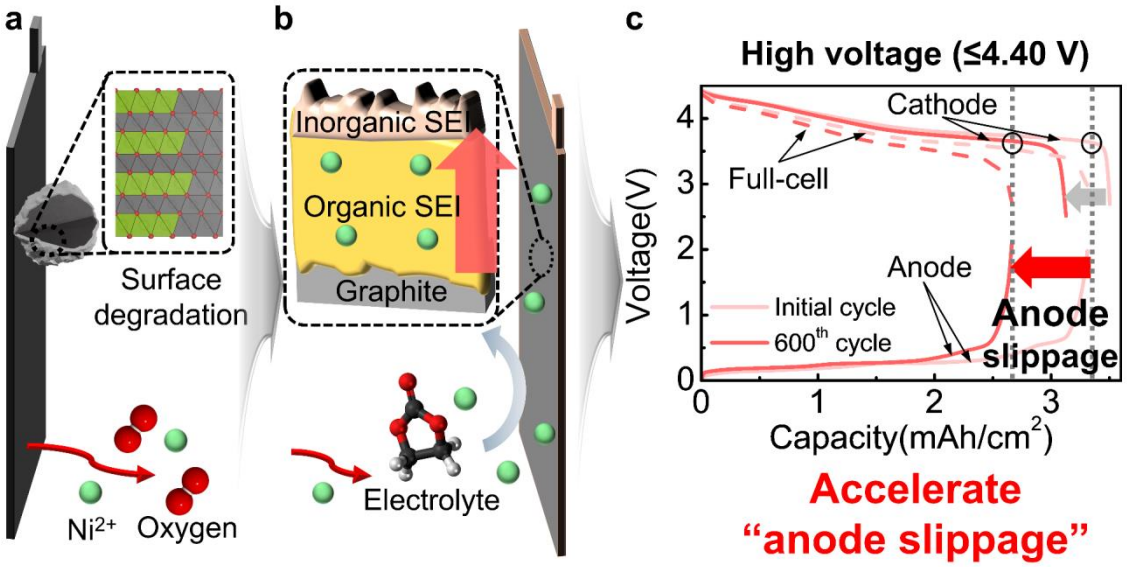

Figure 4. Schematic illustration of SC-NCM6/graphite degradation mechanism operating at high voltage: (a) Cathode surface degradation accompanied by oxygen loss and nickel ion dissolution. (b) Anode surface degradation induced by dissolved Ni ions from the cathode. (c) Occurrence of anode slippage and full cell capacity loss. Red and grey arrows indicate the amount of the capacity induced by the anode slippage and cathode degradation each.

Author contribution statement

Seungjae Suk: methodology, conceptualization, investigation, visualization, validation, and writing the original draft; Namgu Yoo: methodology, conceptualization, visualization, and review; Youngsu Lee, Jasub Kwon: methodology, investigation and review; Heeju Ahn, Seungsu Yoo, Jaewoon Lee, Haneul Kim, Joongho Bae, Jongwoo Kim, Chiho Jo: resources, validation, and review; Yong-Tae Kim: resources; Kyu-Young Park: conceptualization, resources, writing – review & editing, supervising and funding acquisition.

Impact statement

This study identifies cross-talk–induced anode slippage as the dominant degradation mechanism in high-voltage mid-Ni NCM/graphite full-cells, emphasizing the need for mechanistic understanding for rational design of durable high-voltage systems.

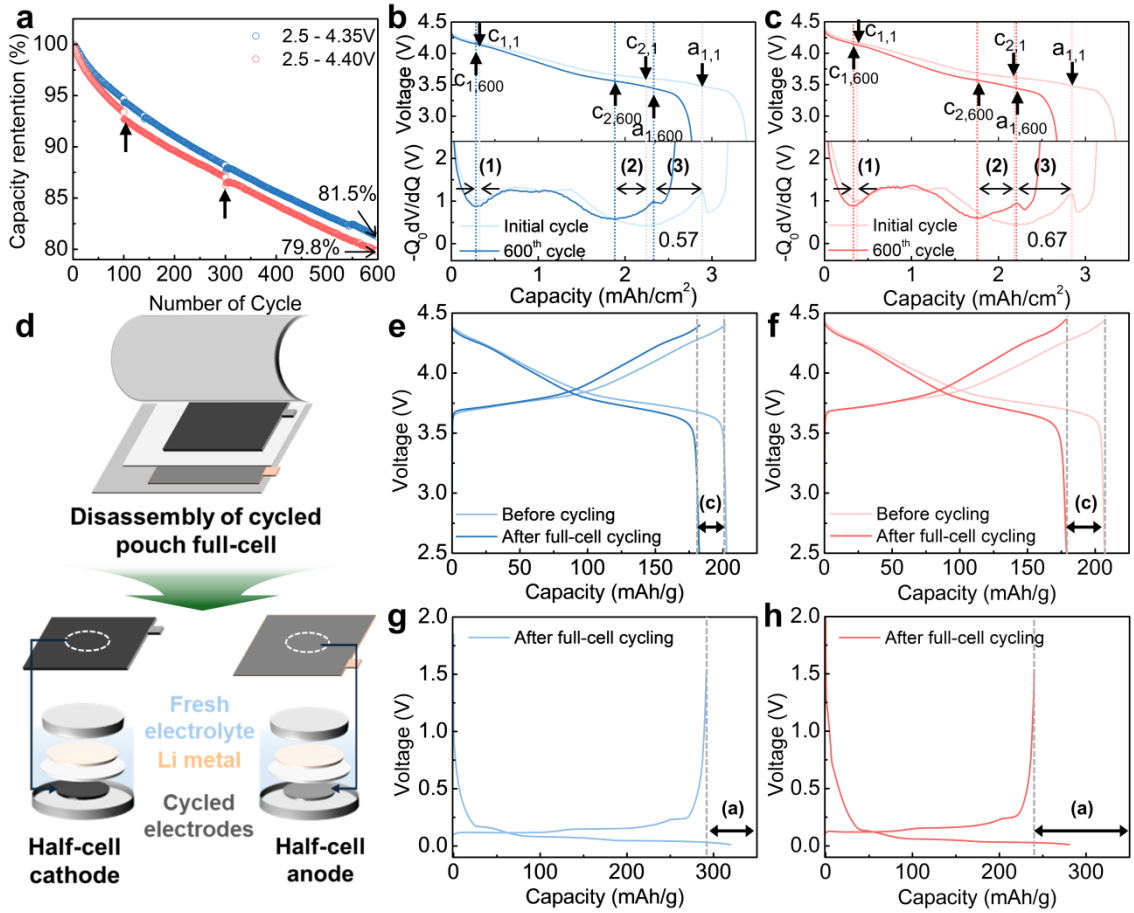

Figure 1

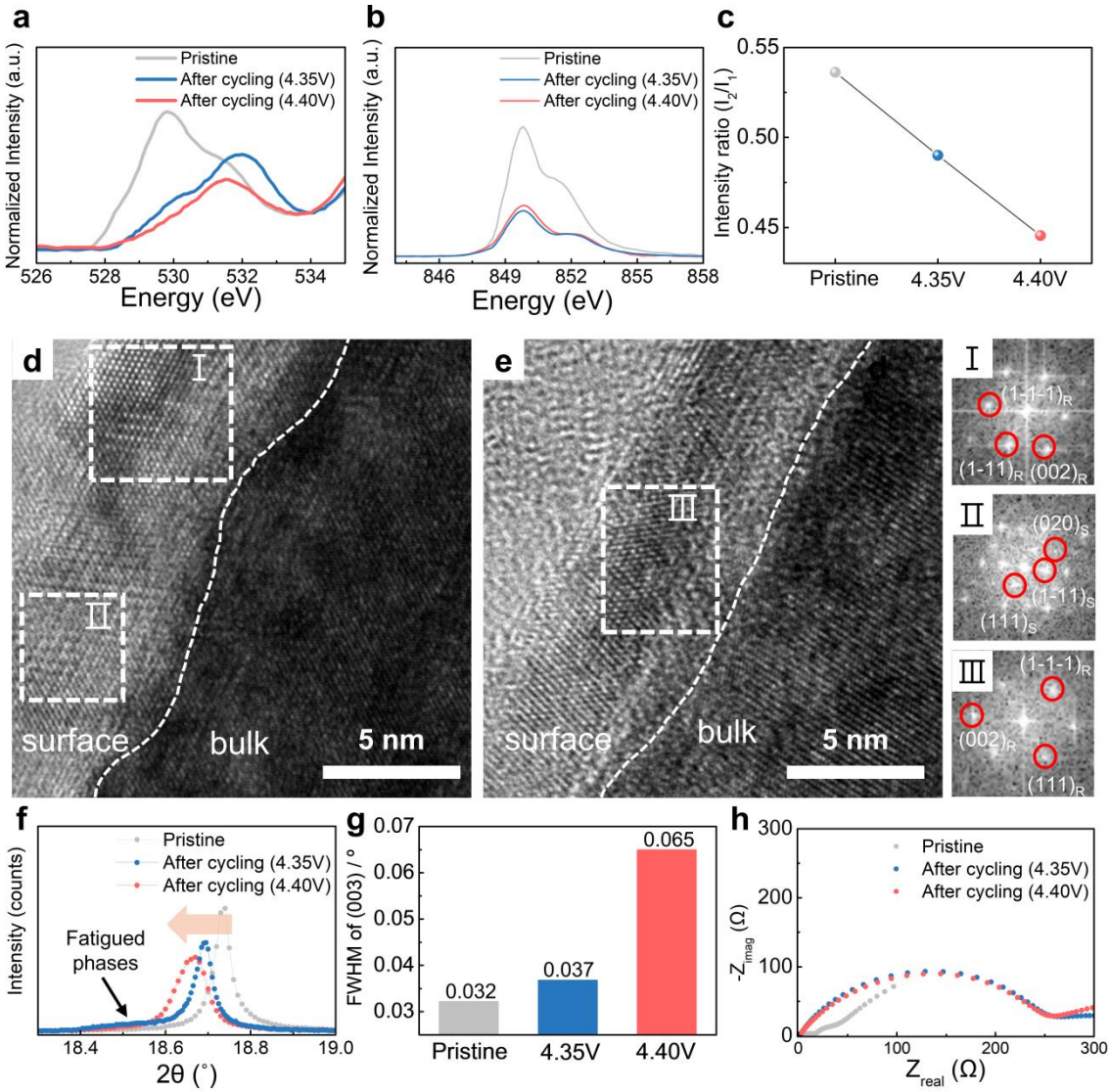

Figure 2

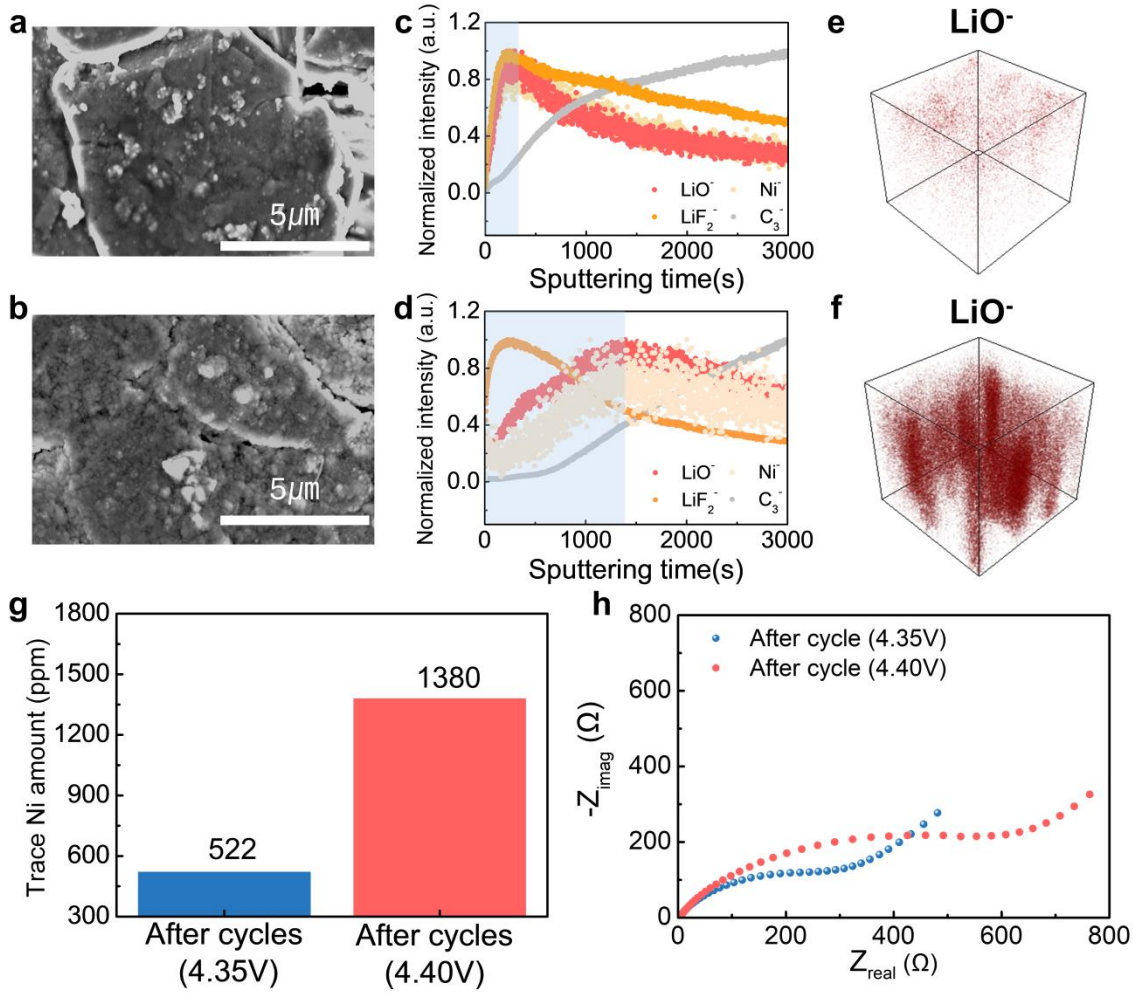

Figure 3

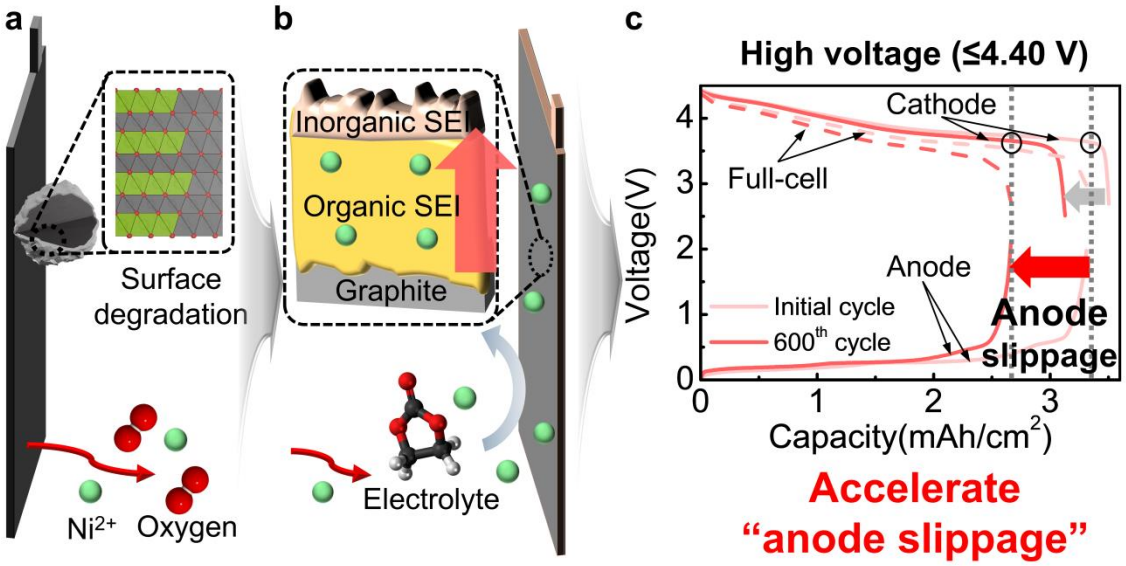

Figure 4

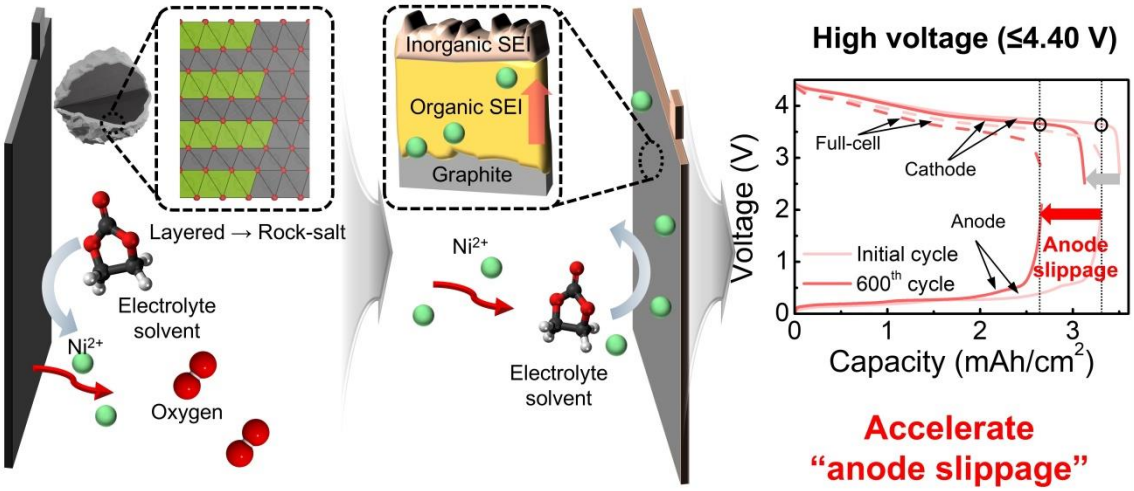

GraphicalAbstract

Supporting Information

Understanding cross-talk–induced anode slippage in high-voltage mid-Ni NCM/graphite full cells

Seungjae Suk[a], Namgyu Yoo[b], Youngsu Lee[b], Jaesub Kwon[a], Heeju Ahn[c], Seungsu Yoo[c], Jaewoon Lee[d], Haneul Kim[c], Joongho Bae[c], Jongwoo Kim[c], Chiho Jo[c], Young-Tae Kim[a] and Kyu-Young Park[a,b*]

[a]*Department of Materials Science and Engineering, Pohang University of Science and Technology (POSTECH), Pohang 37673, Republic of Korea.*

[b]*Graduate Institute of Ferrous & Eco Materials Technology (GIFT), Pohang University of Science and Technology University, Pohang 37666, Republic of Korea*

[c]*LG Energy Solution, Research Park, Daejeon, 34122, Republic of Korea*

[d]*Department of chemical engineering and Materials Science, University of Minnesota–twin cities, Minneapolis, MN 55455, USA*

[*]Dr. Kyu-Young Park,

Assistant Professor of Graduate Institute of Ferrous & Eco Materials Technology

Department of Materials Science and Engineering

Address: 40, Jigok-ro 212beon-gil, Nam-gu, Pohang-si, Gyeongsangbuk-do, Republic of Korea (Zip code: 37667); Mail: kypark0922@postech.ac.kr

ORCID: https://orcid.org/0000-0001-9560-8526

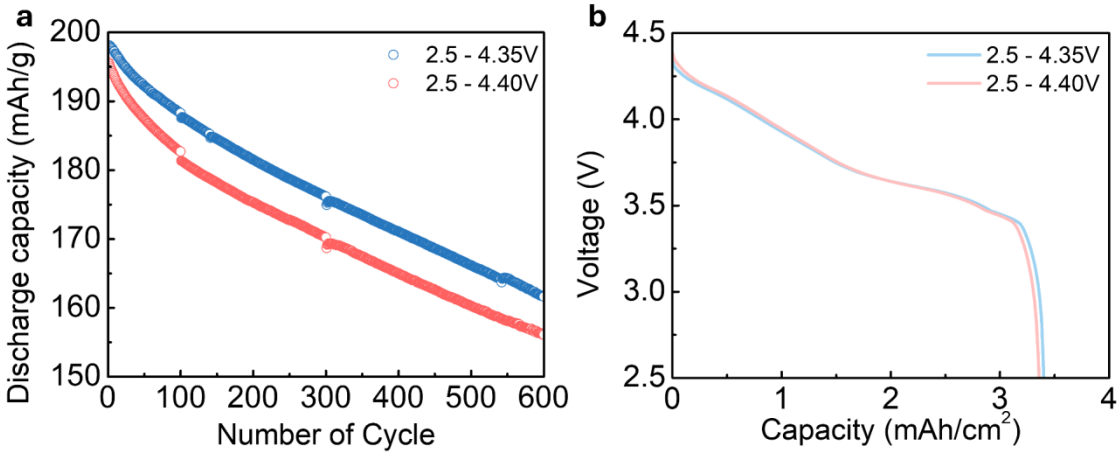

Figure S1. (a)Discharge capacity for the pouch cells cycled at 0.33C between 2.5-4.35 V and 2.5-4.40 V at 45 ℃. (b)Discharge capacity-voltage curve of 1st cycle for each full-cell. Surprisingly, despite the elevated charging voltage of 4.40 V compared to 4.35 V, the full-cell exhibits a reduced initial discharge capacity by 2.5 mAh/g (=0.05 mAh/cm²). A detailed explanation of this phenomenon is provided in Figure S3.

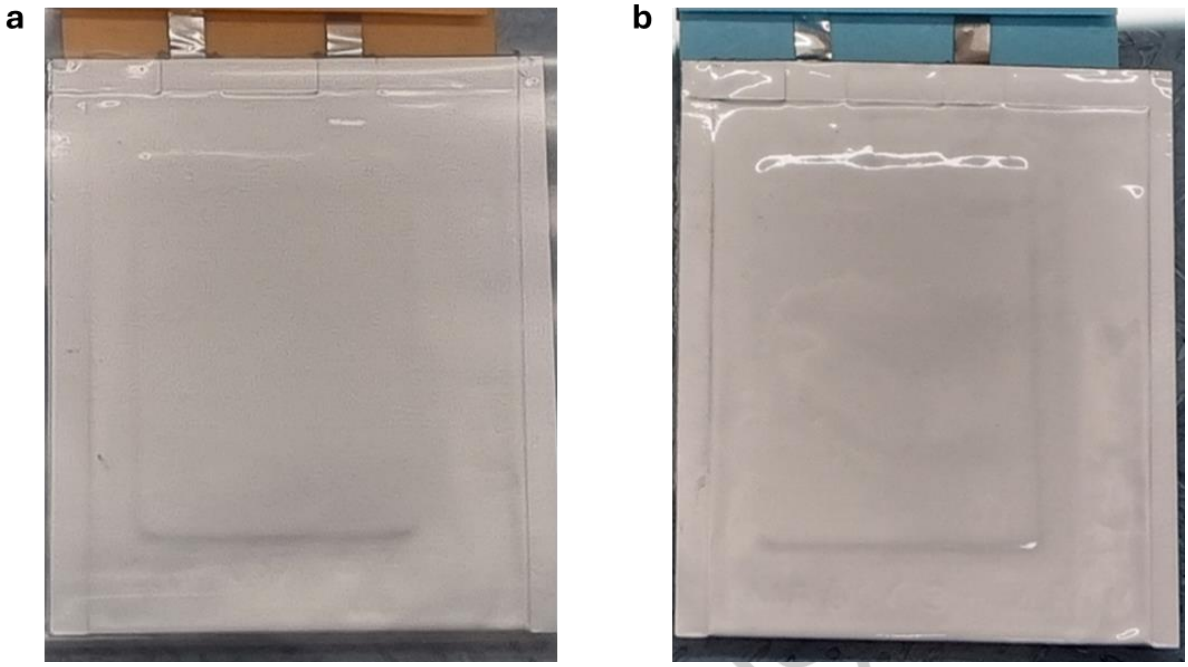

Figure S2. (a) 4.35 V and (b) 4.40 V cycled full-cell appearance after 600 cycles. The full-cell cycled at 4.40 V exhibited slightly greater internal gas accumulation compared to the one cycled at 4.35 V. This difference can be explained by those combined mechanisms: higher voltage operation promoting oxygen release from the cathode surface[4] and electrolyte decomposition.

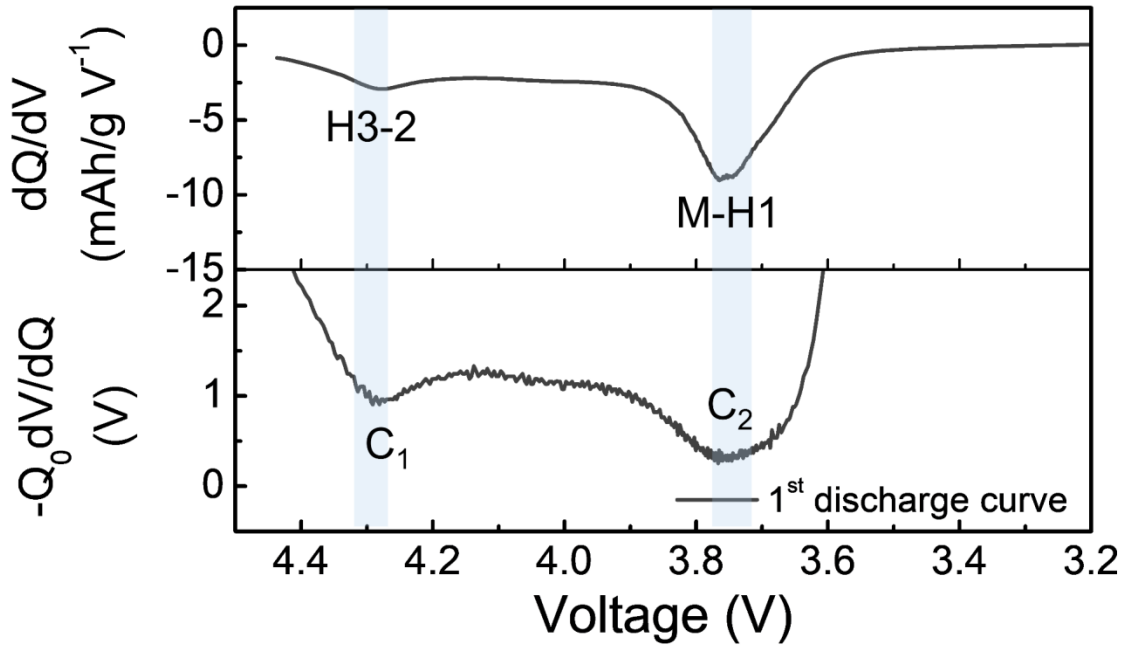

Figure S3. The dQ/dV and $-Q_0dV/dQ$ curves from SC-NCM6 cathode half-cell operated at 2.5-4.40 V (*vs.* Li/Li^+) with 0.3C at 45 °C. In the $-Q_0dV/dQ$ profile, the local minima at ~4.28 V and ~3.76V correspond to two-phase reactions occurring during lithium insertion into SC-NCM6. The phase transition processes are labelled based on previous literature.[1] The 4.28 V minimum is attributed to the H3 to H2 phase transition, while the 3.76 V minimum indicates the coexistence of monoclinic and hexagonal phases.

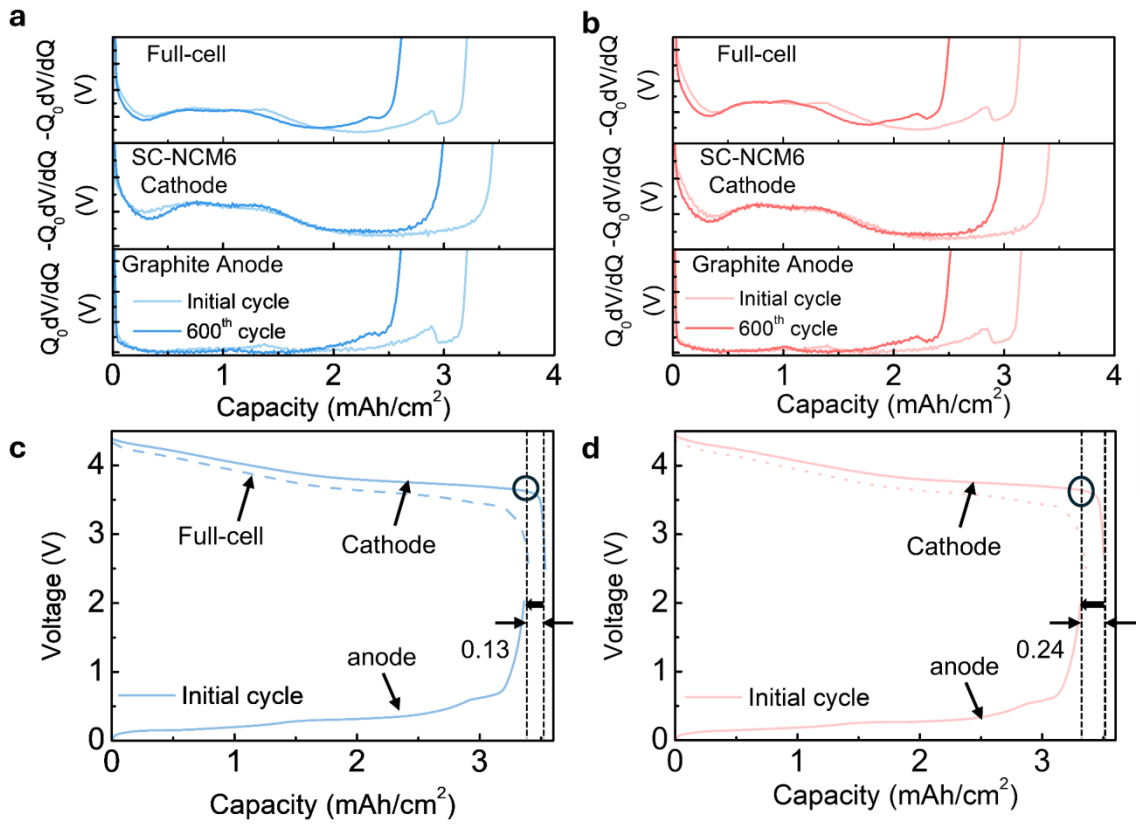

Figure S4. The Q_0dV/dQ curves of the full-cells, SC-NCM6 cathodes and graphite anodes operated at (a) 4.35 V and (b) 4.40 V. The curves for SC-NCM6 were obtained from half-cell experimental data. The anode curves were theoretically derived by subtracting the SC-NCM6 half-cell data from the full-cell data. The galvanostatic curves of the full-cells, cathodes and anodes operated at (c) 4.35 V and (d) 4.40 V based on the full-cell voltage. The black arrows indicate the amount of relative anode slippage after formation.[3] Compared to 4.35 V, slippage occurs 0.11 mAh/cm^2 more at 4.40 V, which leads to lower initial discharge capacity.

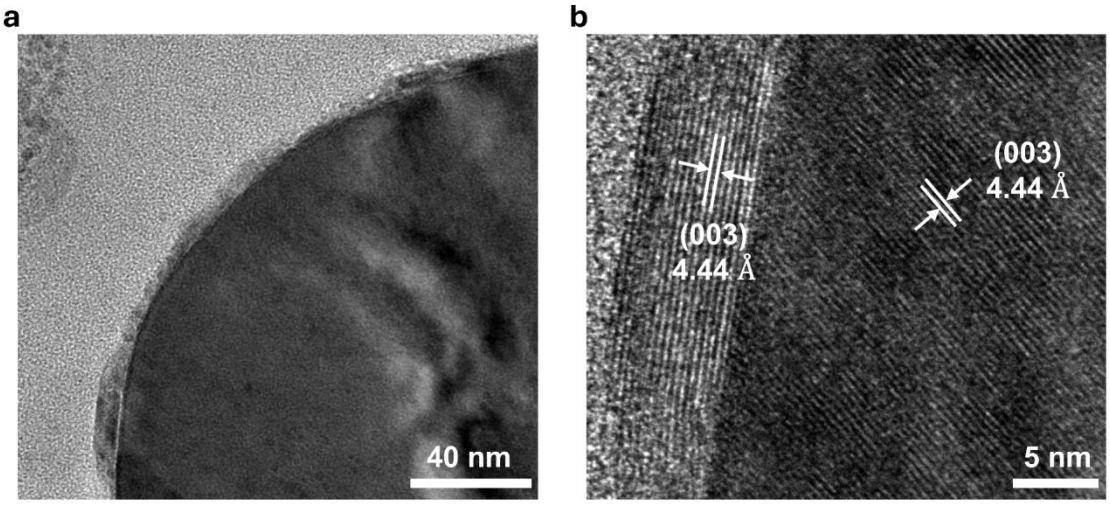

Figure S5. HR-TEM images of the pristine SC-NCM6. (a) HR-TEM visualization at low magnification (b) High-magnification image and the d-spacing value of the nearby surface is 4.44 Å, which indicates the (003) plane of the layered structure ($R\bar{3}m$).

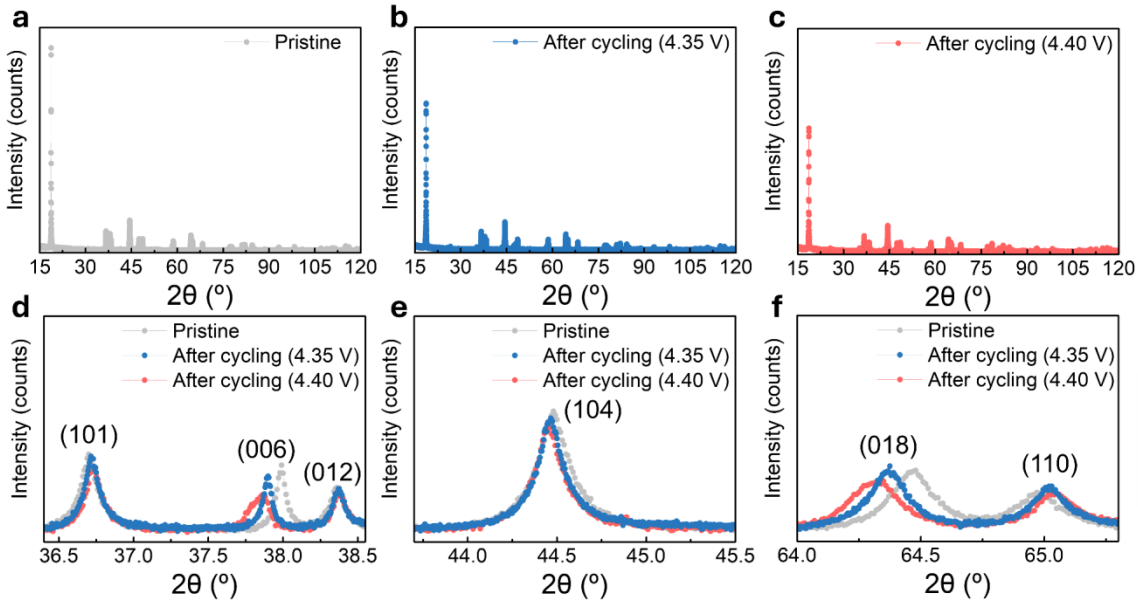

Figure S6. HRPD patterns of (a) pristine SC-NCM6 and electrodes after cycling at (b) 4.35 V and (c) 4.40 V (vs graphite). XRD patterns showing (d) (101), (006), and (012) reflections; (e) (104) reflection; and (f) (018) and (110) reflections.

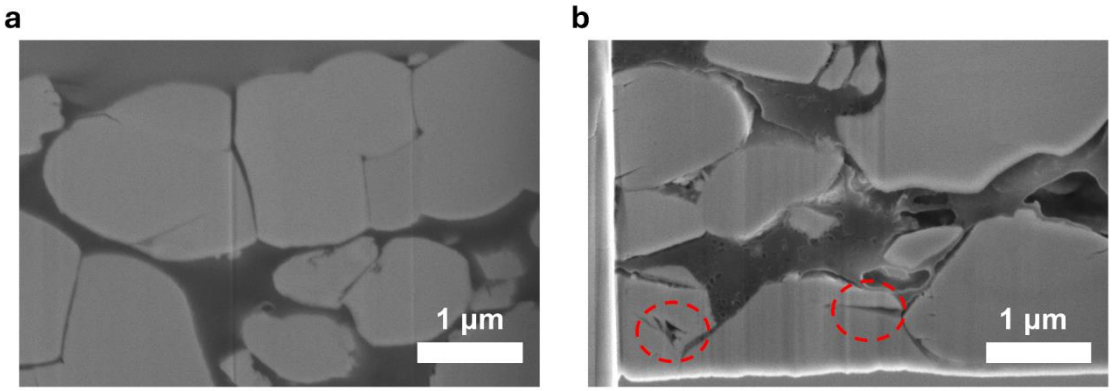

Figure S7. Cross-sectional SEM image of the cycled (a) 4.35 V and (b) 4.40 V SC-NCM6. The red circles indicate the microcracks.

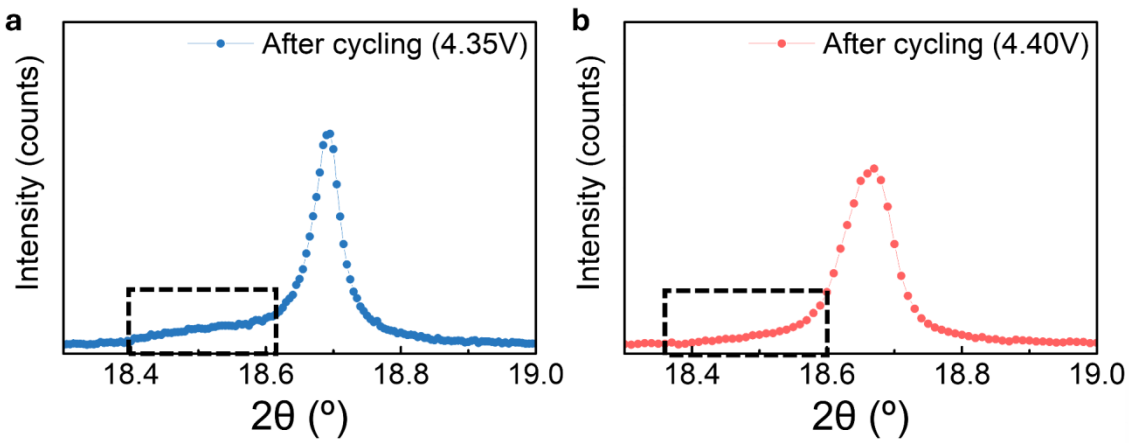

Figure S8. Fatigued phases near the (003) Bragg peak in SC-NCM6 cycled at (a) 4.35 V and (b) 4.40 V. Dotted square box indicates the existence of fatigued phases.

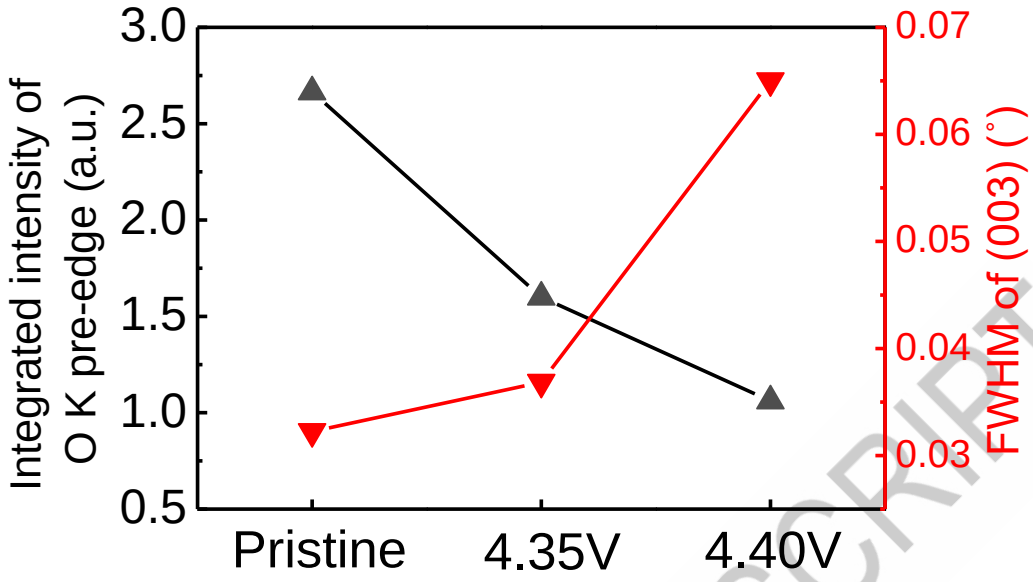

Figure S9. Trend of integrated intensity of O K pre-edge and FWHM of (003) for pristine, 4.35V and 4.40V cycled SC-NCM6. As the areal intensity of O K pre-edge decreases, the FWHM of (003) increases, indicating that surface oxygen release could accelerate bulk degradation.

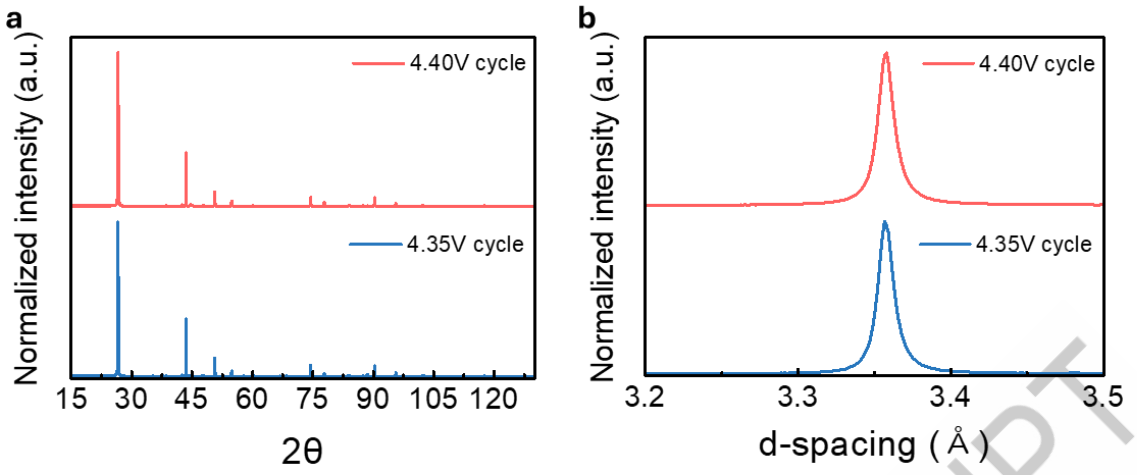

Figure S10. (a) HRPD patterns of graphite anode electrodes after cycling at 4.35 V and 4.40 V (vs graphite). (b) Comparison of d-spacing of the (002) plane for the cycled anode. Analysis of the graphite anodes revealed that the FWHM of the (002) peak measured 0.12075 ˚ and 0.12471 ˚ for samples cycled at 4.35 V and 4.40 V (*vs.* Li/Li+), respectively. The d-spacing values for the (002) plane remained constant at 3.356 Å across both voltage conditions. These findings suggest negligible structural changes in the graphite anode when the upper charging voltage was increased.

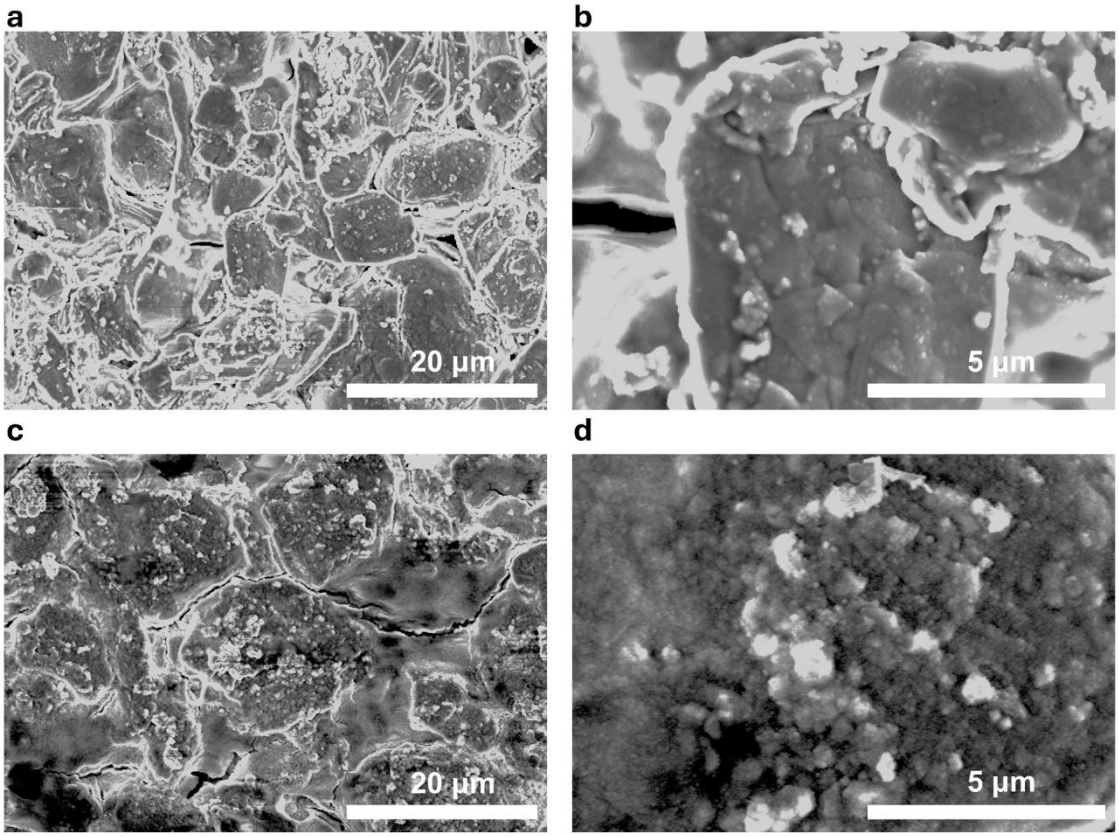

Figure S11. SEM images of graphite electrodes operated at (a,b) 4.35 V and (c,d) 4.40 V cycling.

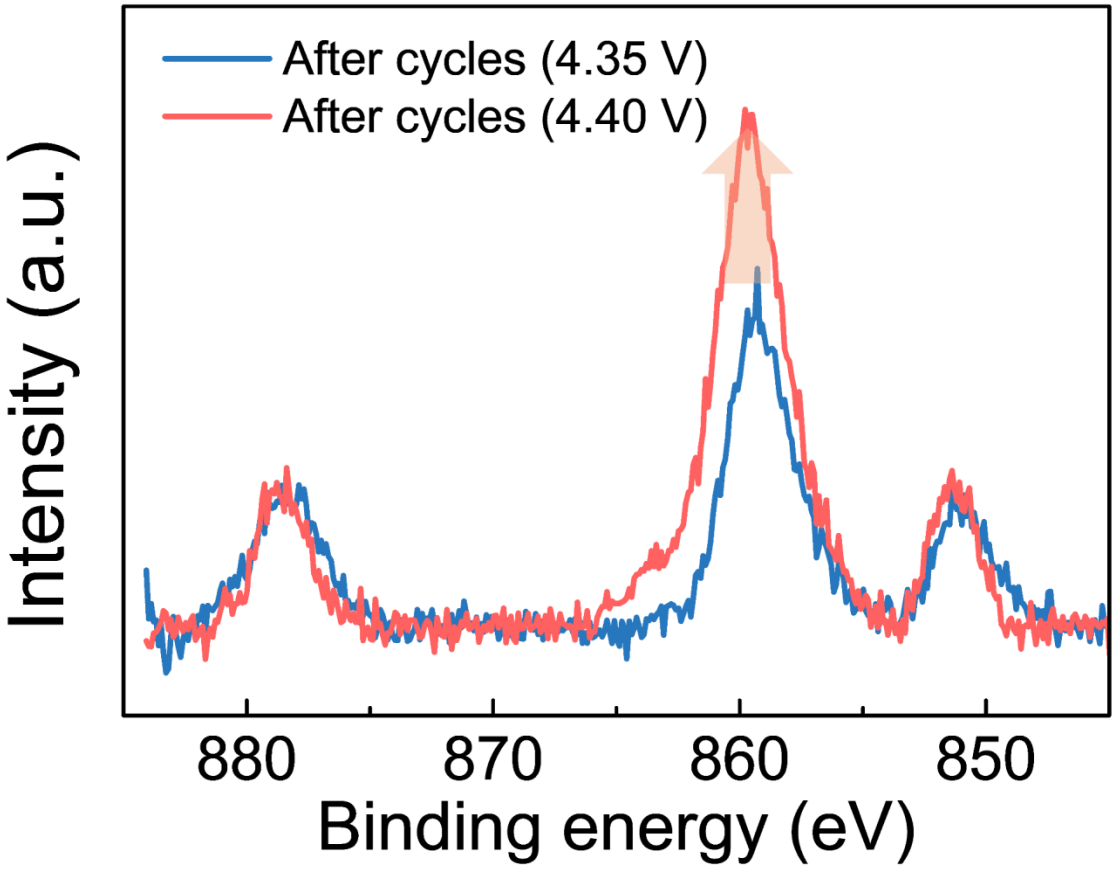

Figure S12. XPS spectra of the cycled graphite anodes. All spectra were obtained after surface etching to eliminate other irrelevant impurities.

Reference

[1] Liu T, Yu L, Liu J, et al. Understanding Co roles towards developing Co-free Ni-rich cathodes for rechargeable batteries. Nat Energy. 2021;6:277–286. doi: 10.1038/s41560-021-00776-y

[2] Ryu HH, Yoon CS, Sun YK, et al. Capacity Fading of Ni-Rich $Li[Ni_xCo_yMn_{1-x-y}]O_2$ ($0.6 \leq x \leq 0.95$) Cathodes for High-Energy-Density Lithium-Ion Batteries: Bulk or Surface Degradation? Chem. Mater. 2018;30:1155–1163. doi: 10.1021/acs.chemmater.7b05269

[3] Gauthier R, Louli, A, Dahn, JR, et al. How do Depth of Discharge, C-rate and Calendar Age Affect Capacity Retention, Impedance Growth, the Electrodes, and the Electrolyte in Li-Ion Cells? J Electrochem Soc. 2022;169(2) doi: 10.1149/1945-7111/ac4b82

[4] Park KY, Zhu YZ, Torres-Castanedo CG, et al. Elucidating and mitigating high-voltage degradation cascades in cobalt-free $LiNiO_2$ lithium-ion battery cathodes. Adv Mater. 2021;34(3). doi: 10.1002/adma.202106402